

VORTEX MATTER IN LOW-DIMENSIONAL SYSTEMS WITH PROXIMITY-INDUCED SUPERCONDUCTIVITY

N. B. Kopnin^{a,b*}, *I. M. Khaymovich*^{c**}, *A. S. Mel'nikov*^c

^a*Lounasmaa Laboratory, Aalto University, P.O. Box 15100
00076, Aalto, Finland*

^b*Landau Institute for Theoretical Physics, Russian Academy of Sciences
117940, Moscow, Russia*

^c*Institute for Physics of Microstructures, Russian Academy of Sciences
603950, Nizhny Novgorod, Russia*

Received April 7, 2013

Dedicated to the memory of Professor Anatoly Larkin

We theoretically study the vortex matter structure in low-dimensional systems with superconducting order induced by proximity to a bulk superconductor. We analyze the effects of microscopic coupling mechanisms between the two systems and the effects of possible mismatch in the band structures of these materials on the energy spectrum of vortex-core electrons. The unusual structure of vortex cores is discussed in the context of recent tunneling microscopy/spectroscopy experiments.

DOI: 10.7868/S0044451013090058

1. INTRODUCTION

The induced superconducting order attracts considerable interest of both theorists and experimentalists for many decades starting from the seminal works on the proximity effect [1, 2]. Recently, we see a revival of this interest, associated with the growing number of experiments carried out for a variety of new artificial systems, which include the two-dimensional electron gas, graphene, semiconducting nanowires and carbon nanotubes, topological insulators, etc. Exotic electronic properties of these systems [3–7] can cause quite unusual manifestations of the proximity effect. Superconducting characteristics of such low-dimensional (LD) systems can differ strongly from those in the bulk. The experiments on proximity-induced superconductivity provide a unique possibility to manipulate the basic properties of the superconducting state. Control of superconducting characteristics can be realized by changing the doping level through the gate potential, which, e. g., creates new types of tunable Josephson

devices [8]. An unconventional gap potential in turn induces unusual quasiparticle (QP) states both in homogeneous and in nonuniform superconducting phases. For LD systems with a nontrivial topological structure, one can possibly realize the QP modes with specific symmetries of the electron and hole wave functions at the Fermi level that describe the so-called Majorana fermions in condensed matter [9, 10].

A standard way of studying the QP states in systems with a complicated superconducting order is to look at the effects of the applied magnetic field on the structure of the mixed state. For example, if the bulk electrode is a type-II superconductor (SC), one can study the structure of vortex lines penetrating the electrode and also threading the LD system (Fig. 1). The goal of this paper is to review the basic properties of the vortex matter formed in the LD layer. A similar problem of vortex matter in the proximity layers naturally arises when one faces the challenge of interpreting the scanning tunneling microscopy/spectroscopy (STM/STS) measurements in SCs. Probing the energy and spatial dependences of the local density of states (LDOS) by STM/STS [11] provides information on the spectrum and the wave functions in the superconducting state. An important part of this information refers

*E-mail: kopnin@boojum.hut.fi

**E-mail: hai@ipm.sci-nnov.ru

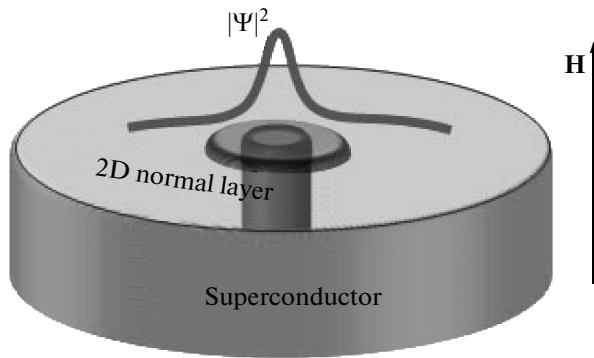


Fig. 1. Sketch of a 2D layer with the multiple vortex core structure induced by a bulk type-II SC in the vortex state. Two scales of the induced vortex are schematically depicted by two small disks in the 2D layer and a cylinder in the bulk superconductor

to the structure of subgap QP states in the magnetic field bound to the vortex core, which are known as the Caroli–de Gennes–Matricon (CdGM) states [12]. A fingerprint of these states is the so-called zero-bias anomaly [11] seen in the STM measurements. A similar anomaly has been observed in contacts of SC and two-dimensional (2D) electron gases with insulating barriers [13] and theoretically described in Refs. [14–17]. Obviously, the intrinsic characteristics of the vortex bound core states can be masked or even hidden by the presence of a thin defect layer at the surface of the bulk SC. In such a thin (possibly nonsuperconducting) surface layer, the superconducting coherence is induced by the proximity to the bulk SC. The masking effect of the defect layer is often difficult to distinguish from more exotic explanations based, e. g., on the assumptions of the superconducting gap anisotropy (see [18, 19] and the references therein) and the multicomponent structure of the order parameter [20, 21]. Despite all its simplicity, the model assuming the presence of a defect layer at the sample surface can explain quite a variety of features in the vortex LDOS experimental data and provides an instructive example of vortex matter in LD systems with the induced superconducting order.

In our studies of vortex matter, instead of considering various phenomenological models of the induced gap potential, we use the general microscopic approach developed in Ref. [22] and focus on the physical mechanisms responsible for formation of the particular gap potential and its symmetry. These mechanisms are mostly determined by the nature of the electron transfer between the 2D proximity system and the bulk SC. This transfer is strongly affected by both the mismatch of the band structures in the coupled subsystems and

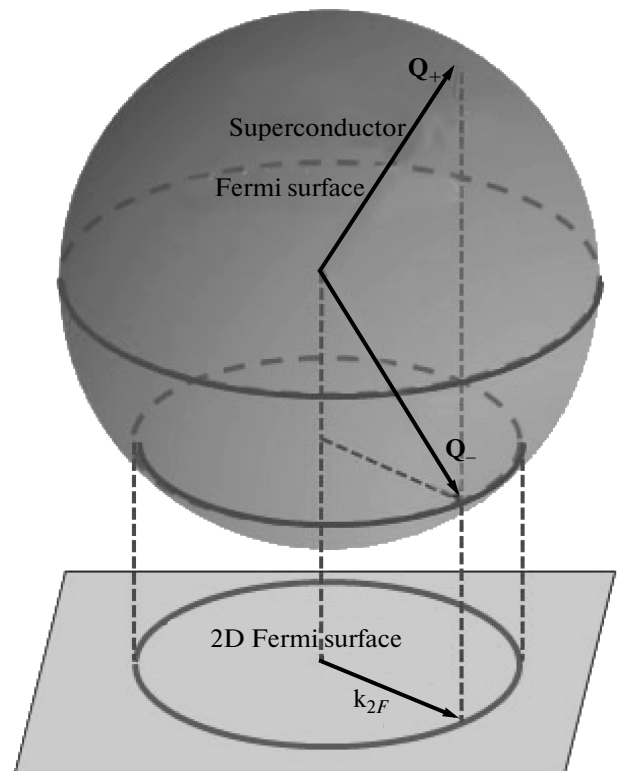


Fig. 2. Matching of Fermi surfaces in the 2D layer and in the bulk superconductor in the coherent tunneling case. In the simple case of isotropic Fermi surfaces, the in-plane projections of the 3D Fermi momenta Q_{\pm} coincide with the Fermi momentum k_{2F} in the 2D layer

by disorder in the barrier between them. Without disorder and neglecting the band structure effects, we arrive at the coherent tunneling model according to which the in-plane projection of the electron momentum is conserved in the course of tunneling. The induced gap potential is determined by matching the 2D Fermi surface with the in-plane projection of the 3D Fermi surface (Fig. 2).

A generalization of the above model can include umklapp processes accounting for the Bloch-type single-electron wave functions in both subsystems. In this last case, the momentum of tunneling electrons is conserved only up to certain vectors of the reciprocal lattices. One more limit case is the so-called incoherent tunneling model, which assumes a strong disorder in the tunneling barrier and allows an arbitrary random change in the momenta of tunneling electrons. The systematic analysis of these three tunneling models shows that the gap potential strongly depends on the degree of disorder as well as on the band structure effects.

Based on these models, we consider several fundamental properties of vortex matter in systems with the induced superconducting order. First, the proximity-induced superconducting gap Δ_{2D} is responsible for the appearance of a new length scale in the vortex structure, the 2D coherence length $\xi_{2D} = \hbar v_{2F}/\Delta_{2D}$ or $\xi_{2D} = \sqrt{\hbar D_{2D}/\Delta_{2D}}$ for clean or dirty limits, respectively. Here, v_{2F} and D_{2D} are the Fermi velocity and diffusion constant in the 2D layer. The energy gap Δ_{2D} depends on the tunneling rate Γ [16, 22–24]; for example, $\Delta_{2D} \approx \Gamma$ for $\Gamma \ll \Delta$. Since $\Delta_{2D} \ll \Delta$, the coherence length ξ_{2D} is usually much longer than the coherence length in the bulk SC, $\xi_S = \hbar v_F/\Delta$ for the clean or $\xi_S = \sqrt{\hbar D_S/\Delta}$ for the dirty limit, where Δ , v_F , and D_S are the gap, the Fermi velocity, and the diffusion constant in the superconducting electrode. As a result, all the effects associated with overlapping of neighboring vortex cores as well as the normal QP scattering at the boundary of the 2D system become much more pronounced than in the primary superconducting electrode. There appears, e. g., an intriguing possibility to obtain a new type of vortex matter strongly bonded by the intervortex QP tunneling even for magnetic fields well below the upper critical field of the bulk SC.

Second, hybridization of the localized QP states inside much larger induced vortex cores with the core states of primary vortices in the bulk electrode leads to a peculiar structure of the subgap energy branches. For coherent tunneling, the electronic spectrum of a singly quantized vortex consists of two anomalous branches crossing the zero energy value as functions of the impact parameter b . One branch, $\epsilon_1(b)$, qualitatively follows the usual CdGM spectrum $\epsilon_0(b)$ of the primary vortex; it extends above the induced gap, where it turns into a scattering resonance. The other branch, $\epsilon_2(b)$, lies below the induced gap and resembles the CdGM spectrum for a vortex with a much larger core radius of the order of ξ_{2D} . Hence, the proximity-induced vortex in a ballistic 2D layer has a “multiple core” structure characterized by the two length scales, ξ_S and ξ_{2D} . Such a two-scale feature does not appear if the proximity vortex states are induced by a primary vortex pinned at a large-size hollow cylinder $r_0 > \xi_S$ (see Refs. [25, 26]).

The spatial and energy dependence of the LDOS inside the multiple core reveals a rich behavior that depends on many parameters and on the degree of disorder both inside the bulk electrode and inside the 2D layer, as well as by the barrier disorder. The barrier disorder suppresses the influence of the primary CdGM spectral branch and leads to broadening of the lower

anomalous branch $\epsilon_2(b)$ due to the momentum uncertainty. Impurity scattering in the bulk and/or inside the 2D layer causes further smearing of the spectral characteristics of the core states, which then approach the usual dirty-SC LDOS scaled with the corresponding coherence lengths ξ_{2D} .

And finally, both the nontrivial topological properties of the normal state wave functions and the induced pairing symmetry can affect the presence of the zero-energy states in the QP spectrum of vortices. This phenomenon arises from the wave function symmetry under precession of the subgap quasiclassical (QC) trajectories inside the vortex core through the corresponding change in the Bohr–Sommerfeld quantization rule for the angular momentum.

The paper is organized as follows. In Sec. 2, we introduce the basic model used in what follows for the analysis of the induced superconductivity. The derivation of self-energies of 2D QC Eilenberger equations in a vortex state of the bulk SC is given in Sec. 3. In Sec. 4, we discuss the method used for the calculation of the subgap state structure in the induced vortex core. The main results are presented in Sec. 5 and 6. In particular, Sec. 5 contains the results for the subgap spectrum and the LDOS in an induced vortex state of a 2D layer. In Sec. 7, we discuss implications of our analysis for induced vortex core states in graphene. We also discuss some further implications of a large value of the induced coherence length ξ_{2D} for the spectral and spatial characteristics of various vortex configurations. Some details of our calculations are given in the Appendix.

2. THE MODEL

We consider a 2D normal metallic layer ($Z = 0$) placed in a tunneling contact with a bulk superconducting half-space $Z > 0$ with a thin insulating barrier between them, as it is shown in Fig. 3. The Hamiltonian of our system has the form $\hat{H} = \hat{H}_S + \hat{H}_{2D} + \hat{H}_T$, where

$$\hat{H}_S = \int d^3R \left[\sum_{\sigma} \hat{\Psi}_{\sigma}^{\dagger}(\mathbf{X}) (\hat{\epsilon}_{3D} - E_F) \hat{\Psi}_{\sigma}(\mathbf{X}) + \Delta(\mathbf{R}) \hat{\Psi}_{\uparrow}^{\dagger}(\mathbf{X}) \hat{\Psi}_{\downarrow}^{\dagger}(\mathbf{X}) + \Delta^*(\mathbf{R}) \hat{\Psi}_{\downarrow}(\mathbf{X}) \hat{\Psi}_{\uparrow}(\mathbf{X}) \right] \quad (1)$$

is the part describing the superconductor with the s -wave order parameter $\Delta(\mathbf{R})$, $\hat{\epsilon}_{3D}$ is the kinetic energy operator,

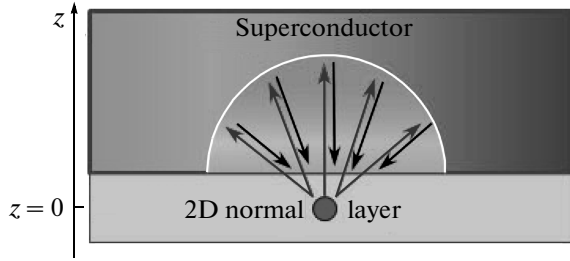


Fig. 3. 2D normal metallic layer ($Z = 0$) coupled to a bulk superconducting half-space $Z > 0$ through a tunneling barrier. The electron waves depicted by gray arrows tunnel from the source placed in the 2D layer (small circle). If the energy is smaller than the superconducting gap, they do not penetrate deep into the bulk superconductor but undergo Andreev reflection to the hole waves (black arrows) and return to the 2D layer

$$\hat{H}_{2D} = d \int d^2r \sum_{\sigma} \hat{a}_{\sigma}^{\dagger}(\mathbf{x}) [\hat{\epsilon}_{2D} - E_F] \hat{a}_{\sigma}(\mathbf{x}) \quad (2)$$

is the 2D-layer Hamiltonian, and d is the thickness of the 2D layer. We introduce space–time variables $\mathbf{X} = (\mathbf{R}, \tau)$ and $\mathbf{x} = (\mathbf{r}, \tau)$, where \mathbf{R} is a three-dimensional vector in the bulk superconducting region and \mathbf{r} is a two-dimensional vector in the normal layer; τ is an imaginary time variable in the standard Matsubara technique. The chemical potential E_F is supposed to be equal in the subsystems. The single-particle Hamiltonian in the 2D layer, $\hat{\epsilon}_{2D}$, includes the kinetic energy and, in general, the lattice potential corresponding to the crystal structure of the normal system. For simplicity, we neglect the band structure of the bulk superconductor. This approximation should be valid for a wide class of heterostructures where the Fermi surface in the bulk SC is large compared with that in the 2D layer. We assume that tunneling is spin-independent and occurs locally in time and in space, i. e., from a point near the interface $\mathbf{R} = (\mathbf{r}, Z = 0)$ on the superconductor side into the point \mathbf{r} in the layer and back with the amplitude $t(\mathbf{r})$ that depends on the coordinate of the tunneling center on the interface. Because the tunneling amplitude accounts for a certain region of an atomic size in the vicinity of the tunneling center, the wave function magnitude at $Z = 0$ should be regarded as an average value near the exact boundary of the superconducting region. The tunneling amplitude is assumed small in the atomic scale. More detailed restrictions on the value of the tunneling amplitude are discussed below. The tunneling Hamiltonian has the form

$$\hat{H}_T = d \sum_{\sigma} \int \left[t(\mathbf{r}) \hat{\Psi}_{\sigma}^{\dagger}(\mathbf{x}) a_{\sigma}(\mathbf{x}) + t^*(\mathbf{r}) \hat{a}_{\sigma}^{\dagger}(\mathbf{x}) \hat{\Psi}_{\sigma}(\mathbf{x}) \right] d^2r, \quad (3)$$

where the wave functions in the superconductor are taken at the space–time point \mathbf{x} at the interface $Z = 0$.

The Matsubara Green’s functions take the form

$$\begin{aligned} \langle T_{\tau} \hat{a}_{\alpha}(\mathbf{x}_1) \hat{a}_{\beta}^{\dagger}(\mathbf{x}_2) \rangle &= \delta_{\alpha\beta} G(\mathbf{x}_1, \mathbf{x}_2), \\ \langle T_{\tau} \hat{\Psi}_{\alpha}(\mathbf{X}_1) \hat{a}_{\beta}^{\dagger}(\mathbf{x}_2) \rangle &= \delta_{\alpha\beta} G_T(\mathbf{X}_1, \mathbf{x}_2), \\ \langle T_{\tau} \hat{\Psi}_{\alpha}(\mathbf{X}_1) \hat{\Psi}_{\beta}^{\dagger}(\mathbf{X}_2) \rangle &= \delta_{\alpha\beta} G_S(\mathbf{X}_1, \mathbf{X}_2), \end{aligned} \quad (4)$$

and

$$\begin{aligned} \langle T_{\tau} \hat{a}_{\alpha}(\mathbf{x}_1) \hat{a}_{\beta}(\mathbf{x}_2) \rangle &= i \hat{\sigma}_{\alpha\beta}^{(y)} F(\mathbf{x}_1, \mathbf{x}_2), \\ \langle T_{\tau} \Psi_{\alpha}(\mathbf{X}_1) \hat{a}_{\beta}(\mathbf{x}_2) \rangle &= i \hat{\sigma}_{\alpha\beta}^{(y)} F_T(\mathbf{X}_1, \mathbf{x}_2), \\ \langle T_{\tau} \hat{\Psi}_{\alpha}(\mathbf{X}_1) \hat{\Psi}_{\beta}(\mathbf{X}_2) \rangle &= i \hat{\sigma}_{\alpha\beta}^{(y)} F_S(\mathbf{X}_1, \mathbf{X}_2), \end{aligned} \quad (5)$$

etc. Equations for the Green’s functions can be more conveniently written in the frequency representation $\omega_n = (2n + 1)\pi T$. We set $\tau = \tau_1 - \tau_2$ and write

$$G(\mathbf{r}_1, \mathbf{r}_2) = \int_0^{\hbar/T} G(\mathbf{r}_1, \mathbf{r}_2; \tau) \exp\left(\frac{i\omega_n \tau}{\hbar}\right) d\tau$$

omitting the subscript for simplicity. We also introduce the Nambu matrices for the Hamiltonian and for the Green’s functions,

$$\check{H}_S = \begin{pmatrix} \hat{\epsilon}_{3D} - E_F & -\Delta(\mathbf{R}) \\ \Delta^*(\mathbf{R}) & \hat{\epsilon}_{3D} - E_F \end{pmatrix}, \quad \check{G} = \begin{pmatrix} G & F \\ -F^{\dagger} & \check{G} \end{pmatrix},$$

and the inverse operators

$$\check{G}_S^{-1}(\mathbf{R}) = -i\check{\tau}_3\omega_n + \check{H}_S,$$

$$\check{G}_{2D}^{-1}(\mathbf{r}) = -i\check{\tau}_3\omega_n + \check{\tau}_0 \otimes [\hat{\epsilon}_{2D} - E_F]$$

in the SC and in the 2D layer, respectively. Here, $\check{\tau}_i$ are the Pauli matrices in the Nambu space.

Equations for the mixed Green’s functions $\check{G}_T(\mathbf{R}_1, \mathbf{r}_2)$ can be written in the form

$$\check{G}_S^{-1}(\mathbf{R}_1) \check{G}_T(\mathbf{R}_1, \mathbf{r}_2) + d\check{t}(\mathbf{R}_{1\perp}) \check{G}(\mathbf{R}_{1\perp}, \mathbf{r}_2) \delta(Z_1) = 0,$$

where $Z_1 \geq 0$, $\mathbf{R}_1 = (\mathbf{R}_{1\perp}, Z_1)$ and

$$\check{t}(\mathbf{r}) = \begin{pmatrix} t(\mathbf{r}) & 0 \\ 0 & t^*(\mathbf{r}) \end{pmatrix}.$$

Neglecting the back-action of a thin 2D layer on the superconductor, we assume that the superconducting Green's function $\check{G}_S(\mathbf{R}_1, \mathbf{R}_2)$ is the noninteracting function that satisfies

$$\check{G}_S^{-1}(\mathbf{R}_1)\check{G}_S(\mathbf{R}_1, \mathbf{R}_2) = \check{1}\hbar\delta(\mathbf{R}_1 - \mathbf{R}_2) \quad (6)$$

in the range $Z_{1,2} > 0$. The function $\check{G}_S(\mathbf{R}_1, \mathbf{R}_2)$ satisfies Neumann boundary conditions at $Z = 0$. This gives

$$\check{G}_T(\mathbf{R}_1, \mathbf{r}_2) = -\frac{d}{\hbar} \int \check{G}_S(\mathbf{R}_1, \mathbf{r}')\check{t}(\mathbf{r}')\check{G}(\mathbf{r}', \mathbf{r}_2) d^2r'. \quad (7)$$

Equations for the Green's functions in the layer can be written as

$$\begin{aligned} \check{G}_{2D}^{-1}(\mathbf{r}_1)\check{G}(\mathbf{r}_1, \mathbf{r}_2) + \check{t}^*(\mathbf{r}_1)\check{G}_T(\mathbf{r}_1, \mathbf{r}_2) = \\ = \check{1}\hbar d^{-1}\delta(\mathbf{r}_1 - \mathbf{r}_2). \end{aligned}$$

Using Eq. (7), we find

$$\begin{aligned} \check{G}_{2D}^{-1}(\mathbf{r}_1)\check{G}(\mathbf{r}_1, \mathbf{r}_2) - \int \check{\Sigma}_T(\mathbf{r}_1, \mathbf{r}')\check{G}(\mathbf{r}', \mathbf{r}_2) d^2r' = \\ = \check{1}\hbar d^{-1}\delta(\mathbf{r}_1 - \mathbf{r}_2), \quad (8) \end{aligned}$$

where

$$\begin{aligned} \check{\Sigma}_T(\mathbf{r}_1, \mathbf{r}') = \begin{pmatrix} \Sigma_1 & \Sigma_2 \\ -\Sigma_2^\dagger & \bar{\Sigma}_1 \end{pmatrix} = \\ = \frac{d}{\hbar}\check{t}^*(\mathbf{r}_1)\check{G}_S^0(\mathbf{r}_1, \mathbf{r}')\check{t}(\mathbf{r}'). \quad (9) \end{aligned}$$

We introduce the momentum representation of the Green's function [27],

$$\begin{aligned} \check{G}_S(\mathbf{R}_1, \mathbf{R}_2) = \int \frac{d^3Q_1}{(2\pi)^3} \frac{d^3Q_2}{(2\pi)^3} \check{G}_S(\mathbf{Q}_1, \mathbf{Q}_2) \times \\ \times \exp(i\mathbf{Q}_1 \cdot \mathbf{R}_1 - i\mathbf{Q}_2 \cdot \mathbf{R}_2), \quad (10) \end{aligned}$$

and of the tunneling coefficients

$$\check{t}(\mathbf{r}) = \int \frac{d^2q}{(2\pi)^2} \check{t}(\mathbf{q})e^{i\mathbf{q} \cdot \mathbf{r}}.$$

The Fourier representation for the Green's functions in the 2D layer is

$$\begin{aligned} \check{G}(\mathbf{r}_1, \mathbf{r}_2) = \int \frac{d^2q_1}{(2\pi)^2} \frac{d^2q_2}{(2\pi)^2} \check{G}(\mathbf{q}_1, \mathbf{q}_2) \times \\ \times \exp(i\mathbf{q}_1 \cdot \mathbf{r}_1 - i\mathbf{q}_2 \cdot \mathbf{r}_2). \quad (11) \end{aligned}$$

2.1. Tunneling with umklapp processes

The crystal structure of the 2D layer accounts for an atomic-scale periodic potential in Eq. (8), which mixes the Fourier harmonics with the momenta shifted by the reciprocal lattice vectors \mathbf{b} . Using the Bloch functions

$$\psi_m(\mathbf{k}, \mathbf{r}) = \sum_{\mathbf{b}} e^{i(\mathbf{k}+\mathbf{b}) \cdot \mathbf{r}} u_{m\mathbf{k}+\mathbf{b}}$$

that diagonalize the single-particle energy operator inside the layer,

$$\epsilon_{2D}(\mathbf{r})\psi_m(\mathbf{k}, \mathbf{r}) = \epsilon_m(k)\psi_m(\mathbf{k}, \mathbf{r}),$$

we can conveniently introduce the field operators $\hat{a}_{\alpha,m,\mathbf{k}}$:

$$\hat{a}_\alpha(\mathbf{r}) = \sum_m \int \frac{d^2k}{(2\pi)^2} \hat{a}_{\alpha,m,\mathbf{k}}\psi_m(\mathbf{k}, \mathbf{r}).$$

The index m enumerates the energy bands.

Introducing the corresponding Green's functions

$$\begin{aligned} \langle T_\tau \hat{a}_{\alpha,m_1,\mathbf{k}_1} \hat{a}_{\beta,m_2,\mathbf{k}_2}^\dagger \rangle = \delta_{\alpha\beta} G_{m_1,m_2}(\mathbf{k}_1, \mathbf{k}_2), \\ \langle T_\tau \hat{a}_{\alpha,m_1,\mathbf{k}_1} \hat{a}_{\beta,m_2,-\mathbf{k}_2} \rangle = i\hat{\sigma}_{\alpha\beta}^{(y)} F_{m_1,m_2}(\mathbf{k}_1, \mathbf{k}_2) \end{aligned} \quad (12)$$

allows diagonalizing the operator \check{G}_{2D}^{-1} in Eq. (8) in the Bloch representation,

$$\begin{aligned} \check{G}_{2D,m}^{-1}(\mathbf{k}) = -i\hbar\check{\tau}_3\omega_n + \\ + \begin{pmatrix} \epsilon_m(\mathbf{k}) - E_F & 0 \\ 0 & \epsilon_m(-\mathbf{k}) - E_F \end{pmatrix}. \quad (13) \end{aligned}$$

We assume in what follows that the amplitude Δ_{ind} of the induced superconducting gap Δ_{2D} is small compared with the interband distance $\epsilon_m - \epsilon_{m'}$ and neglect the interband scattering. Hereafter, we omit the subscripts m . At the same time, the transformation from the momentum to the quasimomentum representation results in a mixing of Fourier harmonics in the self-energy in Eq. (8). Finally, Eq. (8) for Green's functions (12) takes the form

$$\begin{aligned} \check{G}_{2D}^{-1}(\mathbf{k}_1)\check{G}(\mathbf{k}_1, \mathbf{k}_2) - \int \check{\Sigma}_T(\mathbf{k}_1, \mathbf{k}')\check{G}(\mathbf{k}', \mathbf{k}_2) d^2k' = \\ = \check{1}\hbar\delta(\mathbf{k}_1 - \mathbf{k}_2), \quad (14) \end{aligned}$$

with

$$\begin{aligned} \check{\Sigma}_T(\mathbf{k}_1, \mathbf{k}') = \frac{d}{\hbar} \int \check{t}_b^\dagger(\mathbf{k}_1, \mathbf{Q}_\perp) \times \\ \times \check{G}_S^0(\mathbf{Q}, \mathbf{Q}')\check{t}_b(\mathbf{Q}'_\perp, \mathbf{k}') d^3Q d^3Q', \end{aligned}$$

$$\check{t}_b(\mathbf{Q}, \mathbf{k}) = \sum_{\mathbf{b}} u_{\mathbf{k}+\mathbf{b}} \check{t}(\mathbf{Q}_\perp - \mathbf{k} - \mathbf{b}) \quad (15)$$

and $\check{t}_b^\dagger(\mathbf{k}, \mathbf{Q}_\perp) = \check{t}_b^*(\mathbf{Q}_\perp, \mathbf{k})$. Here, $\mathbf{Q} = (\mathbf{Q}_\perp, Q_z)$. The above expression for the tunneling coefficients t_b in fact describes the umklapp processes caused by the periodic crystal potential in the 2D layer.

2.2. Coherent tunneling

The simplest model of tunneling assumes that the in-plane momentum projection of electrons is conserved during the tunneling process:

$$\check{t}(\mathbf{Q}_\perp - \mathbf{k}) = \check{t}\delta(\mathbf{Q}_\perp - \mathbf{k}).$$

This is equivalent to the assumption that the tunneling amplitude $t(\mathbf{r})$ is independent of the coordinate along the SC/2D interface. Of course, the quasimomentum conservation is not exact in the presence of energy bands because the tunneling mixes the quasimomentum values that differ by a reciprocal lattice vector:

$$\check{t}_b(\mathbf{Q}, \mathbf{k}) = \check{t} \sum_{\mathbf{b}} u_{\mathbf{k}+\mathbf{b}} \delta(\mathbf{Q}_\perp - \mathbf{k} - \mathbf{b}).$$

Neglecting umklapp processes for simplicity, we find

$$\check{\Sigma}_T(\mathbf{k}_1, \mathbf{k}') = \frac{dt^2}{\hbar} \int \check{G}_S^0(\mathbf{k}_1, Q_z; \mathbf{k}', Q'_z) \frac{dQ_z dQ'_z}{(2\pi)^2}$$

from Eq. (14).

From now on, we use the QC approximation for the Green's functions. To derive the Eilenberger equations in the 2D layer, we follow the standard procedure described, e. g., in Ref. [27]. First, we introduce the average $\mathbf{k} = (\mathbf{k}_1 + \mathbf{k}_2)/2$, $Q_z = (Q_{1z} + Q_{2z})/2$ and relative $\mathbf{k}_- = \mathbf{k}_1 - \mathbf{k}_2$, $q_z = Q_{1z} - Q_{2z}$ momenta and set

$$\check{G}(\mathbf{k}_1, \mathbf{k}_2) = \check{G}(\mathbf{k}, \mathbf{k}_-),$$

$$\check{G}_S(\mathbf{k}_1, Q_{1z}; \mathbf{k}_2, Q_{2z}) = \check{G}_S(\mathbf{k}, Q_z; \mathbf{k}_-, q_z).$$

Next, we apply the operator \check{G}_{2D}^{-1} to the Green's function $\check{G}(\mathbf{k}, \mathbf{k}_-)$ from the right and subtract this equation from Eq. (14). We now transform to the semiclassical Green's functions by integrating the resulting equation over $d\xi_2$, where $\xi_2 = \epsilon_{2D}(\mathbf{k}) - E_F$. The Green's functions are to be taken in the vicinity of the Fermi surface. Therefore, in the mixed momentum-coordinate representation,

$$\check{G}(\mathbf{k}, \mathbf{r}) = \int \check{G}(\mathbf{k}, \mathbf{k}_-) \exp(i\mathbf{k}_- \cdot \mathbf{r}) \frac{d^2k_-}{(2\pi)^2},$$

$$\check{G}_S(\mathbf{k}, Q_z; \mathbf{r}, Z) = \int \check{G}_S(\mathbf{k}, Q_z; \mathbf{k}_-, q_z) \times \exp(i\mathbf{k}_- \cdot \mathbf{r} + iq_z Z) \frac{d^2k_- dQ_z}{(2\pi)^3},$$

we can put

$$\check{G}_S(\mathbf{k}, Q_z; \mathbf{r}, Z) = \check{g}_S(\mathbf{k}, Q_z; \mathbf{r}, Z) \pi i \delta_\Delta(\xi_3),$$

$$\check{G}(\mathbf{k}, \mathbf{r}) = \check{g}(\mathbf{k}, \mathbf{r}) \pi i \delta_\Delta(\xi_2).$$

Here, the standard semiclassical Green's functions are

$$\check{g}(\mathbf{k}_{2F}, \mathbf{r}) = \frac{1}{\pi i} \int d\xi_2 \check{G}(\mathbf{k}, \mathbf{r}), \quad (16)$$

$$\check{g}_S(\mathbf{K}_F, \mathbf{R}) = \frac{1}{\pi i} \int d\xi_3 \check{G}_S(\mathbf{Q}, \mathbf{R}), \quad (17)$$

$\xi_3 = \epsilon_S(\mathbf{Q}) - E_F$ is the normal QP spectrum in the 3D half-space, and $\delta_\Delta(\xi_{2,3})$ is a delta-function broadened at the gap energy scale Δ . The matrix \check{g} is made out of four functions, g, f, f^\dagger , and \bar{g} in the same way the matrix \check{G} is constructed of the functions G, F, F^\dagger , and \bar{G} .

At the next step of derivation, we note that in the mixed representation, the term

$$\int \frac{d\xi_2}{\pi i} \int \check{\Sigma}_T(\mathbf{k}_1, \mathbf{k}') \check{G}(\mathbf{k}', \mathbf{k}_2) \frac{d^2k'}{(2\pi)^2}$$

in the equation for the Green's function becomes

$$\begin{aligned} & \frac{\pi i dt^2}{\hbar} \int d\xi_2 \times \\ & \times \int \frac{dQ_z}{2\pi} \check{g}_S(\mathbf{k}, Q_z; \mathbf{r}, 0) \check{g}(\mathbf{k}, \mathbf{r}) \delta_\Delta(\xi_3) \delta_\Delta(\xi_2) = \\ & = \frac{\pi i dt^2}{\hbar} \int \frac{dQ_z}{2\pi} \check{g}_S(\mathbf{Q}, \mathbf{r}, 0) \check{g}(\mathbf{k}_{2F}, \mathbf{r}) \delta_\Delta[\epsilon_{3D}(\mathbf{Q}) - E_F], \end{aligned}$$

where $\mathbf{Q} = (\mathbf{k}_{2F}, Q_z)$ has the in-plane projection coinciding with the 2D Fermi momentum \mathbf{k}_{2F} .

Finally, we obtain the QC Eilenberger equation for retarded (advanced) Green's functions

$$\begin{aligned} & -i\hbar \mathbf{v}_{2F} \nabla \check{g}(\mathbf{k}_{2F}, \mathbf{r}) - \epsilon [\check{\tau}_3 \check{g}(\mathbf{k}_{2F}, \mathbf{r}) - \check{g}(\mathbf{k}_{2F}, \mathbf{r}) \check{\tau}_3] - \\ & - [\check{\Sigma}_T \check{g}(\mathbf{k}_{2F}, \mathbf{r}) - \check{g}(\mathbf{k}_{2F}, \mathbf{r}) \check{\Sigma}_T] = 0, \quad (18) \end{aligned}$$

where $\hbar \mathbf{v}_{2F} = \partial \epsilon_{2D}(\mathbf{k}) / \partial \mathbf{k}$ is the 2D-layer Fermi velocity.

For isotropic Fermi surfaces in both the SC, $\epsilon_{3D}(\mathbf{Q}) = \hbar^2 Q^2 / 2m$, and the 2D layer, $\epsilon_m(\mathbf{k}) = \hbar^2 k^2 / 2m_{2D}$, the self-energy takes the form

$$\check{\Sigma}_T(\mathbf{k}_{2F}, \mathbf{r}) = \frac{i\Gamma}{2} [\check{g}_S(\mathbf{Q}_+; \mathbf{r}, 0) + \check{g}_S(\mathbf{Q}_-; \mathbf{r}, 0)] \quad (19)$$

with the tunneling rate

$$\Gamma = dt^2 \int_0^\infty \delta_\Delta [\epsilon_S(\mathbf{k}_{2F}, Q_z) - E_F] dQ_z.$$

The 3D momentum $\mathbf{Q}_\pm = (\mathbf{k}_{2F}, \pm Q_{3z})$ lies on the Fermi surface of the bulk SC, $k_{2F}^2 + Q_{3z}^2 = K_F^2$. If the 2D Fermi surface is smaller than the extremal cross section of the 3D Fermi surface, i. e., $k_{2F} < K_F$, the expression for the tunneling rate becomes $\Gamma = dmt^2/Q_{3z}$. For large 2D Fermi surfaces with $k_{2F} > K_F$, the self-energy term vanishes and the coherent tunneling is impossible. The case of momenta $k_{2F} \approx K_F$ deserves special consideration, which should take account of a finite delta-function width $\Gamma \sim dt^2 \sqrt{m/\Delta}$.

The umklapp processes should, of course, modify the self-energy part, resulting in the additional contributions:

$$\check{\Sigma}_T(\mathbf{k}_{2F}, \mathbf{r}) = \sum_{\mathbf{b}} |u_{\mathbf{k}_{2F}+\mathbf{b}}|^2 \check{\Sigma}_T^{(0)}(\mathbf{k}_{2F} + \mathbf{b}, \mathbf{r}), \quad (20)$$

where $\check{\Sigma}_T^{(0)}(\mathbf{k}_{2F}, \mathbf{r})$ is given by Eq. (19).

2.3. Incoherent tunneling

The coherent tunneling model in many cases oversimplifies the realistic experimental situation. The momentum conservation is violated, for example, by the presence of disorder at the interface. Here, we consider an opposite limit of strong disorder, which is sometimes called the incoherent tunneling model. This model assumes a random tunneling process of electrons through the barrier in a way similar to the standard theory of dirty metals within the Born approximation [28]. We assume that the ensemble average of tunneling amplitudes is

$$\overline{t(\mathbf{r}_1)t(\mathbf{r}_2)} = t^2 s_a \delta(\mathbf{r}_1 - \mathbf{r}_2), \quad (21)$$

where s_a is the correlated area of the order of the atomic scale. Following the standard diagrammatic procedure, we expand the solution for the ensemble-averaged Green's function in a series in the scattering field and split the multiple correlators of the $t(\mathbf{r})$ values into a product of the above pair correlators. Finally, after averaging, self-energy (9) becomes

$$\begin{aligned} \check{\Sigma}_T(\mathbf{r}_1, \mathbf{r}_2) &= t^2 ds_a \check{G}_S(\mathbf{r}_1, \mathbf{r}_1; 0) \delta(\mathbf{r}_1 - \mathbf{r}_2) = \\ &= t^2 ds_a i\pi\nu_3(0) \langle \check{g}_S(\mathbf{Q}; \mathbf{r}, 0) \rangle \delta(\mathbf{r}_1 - \mathbf{r}_2), \end{aligned} \quad (22)$$

where $\nu_3(0)$ is the normal density of states in the bulk material. Angular brackets denote averaging over

3D-momentum directions. Within the QC approach, the resulting self-energy to be used in Eilenberger equation (18) is given by

$$\check{\Sigma}_T(\mathbf{r}) = i\Gamma \langle \check{g}_S(\mathbf{Q}; \mathbf{r}, 0) \rangle, \quad (23)$$

where the tunneling rate is $\Gamma = \pi\nu_3(0)ds_at^2$. This approximation coincides with that used in Ref. [22]. The tunneling rate $\Gamma \sim t^2/E_F$ can be expressed [22] in terms of the normal-state tunnel conductance $G = 1/RS$ per unit contact area, $\Gamma = G/4\pi G_0\nu_2 \sim E_FR_0/R$, with the conductance quantum $G_0 = e^2/\pi\hbar$ and the normal 2D density of states (DOS) $\nu_2 = m_{2D}/2\pi\hbar^2$. Therefore, $\Gamma/E_F \ll 1$ if the total tunnel resistance R is much larger than the Sharvin resistance $R_0 = (NG_0)^{-1}$ for an ideal N -mode contact with the contact area S . Nevertheless, there is room for the condition $\Gamma \sim \Delta$ to be fulfilled even for the large contact resistance $R \gg R_0$.

2.4. Adiabatic approximation. Range of validity

The above microscopic analysis allows us to comment on the simplest phenomenological model that is often used in describing the proximity-induced superconductivity (see, e. g., [26, 29–31]). Within this model, the Bogoliubov–de Gennes equations inside the proximity superconductor include a phenomenological gap function, which is postulated to be proportional to the gap function Δ inside the superconducting electrode. Our approach shows that this is generally not the case. The true equation (18) includes self energies that are complicated functions of energy, coordinates, and momentum. In fact, the effective gap function resembles that in the usual superconductor only if the bulk SC is homogeneous in space. In this case, the QC Green's function is

$$\check{g}_\epsilon^{R(A)} = \pm \frac{1}{\sqrt{\epsilon^2 - |\Delta|^2}} \begin{pmatrix} \epsilon & \Delta \\ -\Delta^* & -\epsilon \end{pmatrix}.$$

In this case, the self-energy is $\check{\Sigma}_T = i\Gamma\check{g}_S$ for both coherent and incoherent tunneling models. This expression also holds if the superconducting gap is a slowly varying function of coordinates on distances of the order of ξ_S . For $|\epsilon| < |\Delta|$, the self-energy has the form

$$\check{\Sigma}_T(\mathbf{r}) = \frac{\Gamma}{\sqrt{|\Delta(\mathbf{r})|^2 - \epsilon^2}} \begin{pmatrix} \epsilon & \Delta(\mathbf{r}) \\ -\Delta^*(\mathbf{r}) & -\epsilon \end{pmatrix}. \quad (24)$$

Only for a low-transparency tunnel contact $\Gamma \ll \Delta$, this self-energy is nearly off-diagonal on the scale $\epsilon \sim \Gamma$

and can be regarded as an energy-independent effective gap function

$$\tilde{\Sigma}_T \approx i\Gamma\tilde{\tau}_2 \exp(i\tilde{\tau}_3\phi), \quad (25)$$

where ϕ is the phase of the superconducting order parameter. We note that the resulting induced gap is totally independent of the gap magnitude $|\Delta|$ in the bulk. If the transparency is finite, the electronic spectrum in the induced superconductor has the gap Δ_{2D} determined by the condition [1, 22]

$$(\epsilon + \Sigma_1)^2 - \Sigma_2^2 = 0, \quad \epsilon = \Delta_{2D}. \quad (26)$$

Of course, the adiabatic approximation also breaks down if the order parameter Δ varies as a function of coordinates at distances of the order of the coherence length in the superconducting electrode, when the self-energies are no longer determined by Eq. (24).

3. VORTEX POTENTIALS AND GREEN'S FUNCTIONS FOR CLEAN SYSTEMS

The QC Green's functions in the 2D layer satisfy Eilenberger equations (18). In components,

$$\begin{aligned} -i\hbar v_{2F} \nabla f - 2(\epsilon + \Sigma_1)f + 2\Sigma_2 g &= 0, \\ i\hbar v_{2F} \nabla f^\dagger - 2(\epsilon + \Sigma_1)f^\dagger + 2\Sigma_2^\dagger g &= 0, \\ -i\hbar v_{2F} \nabla g + \Sigma_2 f^\dagger - \Sigma_2^\dagger f &= 0, \end{aligned} \quad (27)$$

and the normalization condition $g^2 - f f^\dagger = 1$ with the self-energies in Eqs. (19) or (23) as effective potentials.

In this and the next sections, we consider the case of isotropic Fermi surfaces. Modifications due to the anisotropy of the spectrum are discussed in Sec. 5.2. Quasiparticles in clean systems are conveniently described by the coordinates along their trajectories (Fig. 4). A QC trajectory is parameterized by its angle α with the x axis, the impact parameter $b = \rho \sin(\phi - \alpha)$, and the coordinate $s = \rho \cos(\phi - \alpha)$ along the trajectory. We introduce the symmetric and antisymmetric parts of the Green's functions as this was done in Refs. [27, 32]:

$$\begin{aligned} f &= -[\zeta(s) + i\theta(s)] e^{i\alpha}, \\ f^\dagger &= [\zeta(s) - i\theta(s)] e^{-i\alpha}, \end{aligned} \quad (28)$$

where $\zeta(s) = \zeta(-s)$ and $\theta(s) = -\theta(-s)$. The normal-

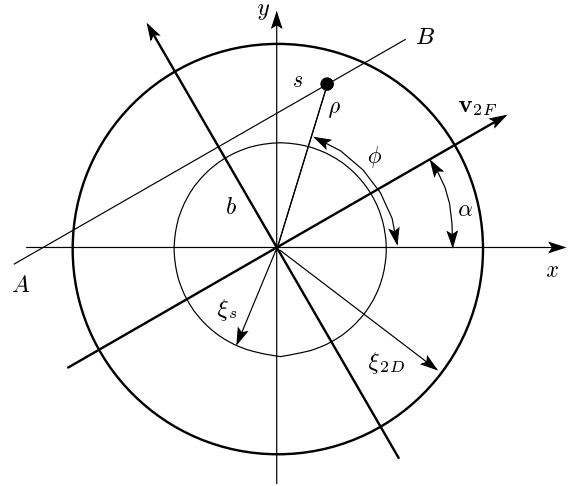


Fig. 4. The coordinate frame near the multiple vortex core. The primary (induced) core is shown by the inner small (outer large) circle. The QC trajectory with an impact parameter b (line AB) passes through the point (ρ, ϕ) shown by the black dot

ization condition requires $g^2 + \theta^2 + \zeta^2 = 1$. Eilenberger equations (27) can be rewritten in the form

$$\hbar v_{2F} \frac{d\zeta}{ds} + 2(\epsilon + \Sigma_1)\theta - 2ig\Sigma_R = 0, \quad (29a)$$

$$\hbar v_{2F} \frac{d\theta}{ds} - 2(\epsilon + \Sigma_1)\zeta - 2ig\Sigma_I = 0, \quad (29b)$$

$$\hbar v_{2F} \frac{dg}{ds} + 2i\zeta\Sigma_R + 2i\theta\Sigma_I = 0, \quad (29c)$$

where

$$\begin{aligned} 2\Sigma_R &= \Sigma_2 e^{-i\alpha} + \Sigma_2^\dagger e^{i\alpha}, \\ 2i\Sigma_I &= \Sigma_2 e^{-i\alpha} - \Sigma_2^\dagger e^{i\alpha}. \end{aligned} \quad (30)$$

In this paper, we consider the limit of low tunneling rate $\Gamma \ll \Delta$, which leads to a small induced gap [22] $\Delta_{2D} = \Gamma$ and long coherence length $\xi_{2D} \gg \xi_S$. We consider an isolated vortex line oriented along the Z axis perpendicular to the SC/2D interface and choose the gap function inside the bulk SC in the form $\Delta = \Delta_0(\rho)e^{i\phi}$, where (ρ, ϕ) are the cylindrical coordinates; $\Delta_0(\rho)$ approaches the bulk value Δ_∞ far from the vortex core. The self-energies in the 2D layer, Eqs. (19) or (23), have parts with sharp peaks localized at small distances $\rho \sim \xi_S$ and the adiabatic long-distance ‘‘vortex potential’’ tail $\Delta_{2D} \sim \Gamma e^{i\phi}$ at $\rho \gg \xi_S$ according to Eq. (25).

In the case of a clean bulk SC, we use the condition of specular reflection at the interface. This can be applied for both coherent and incoherent tunneling models because any possible disorder in tunneling affects only a tiny fraction of bulk electrons, whose vast

majority reflects without tunneling. For specular reflection, we can use the bulk QC Green's functions obtained for an infinite space. For energies $\epsilon \ll \Delta_\infty$, the self-energy in Eq. (25) for long distances ($\rho \gg \xi_S$) is independent of the particular tunneling model and of the disorder in the bulk SC: $\Sigma_1 \approx 0$ and $\Sigma_2 \approx \Gamma e^{i\phi}$, i. e., $\Sigma_R \approx \Gamma s/\rho$ and $\Sigma_I \approx \Gamma b/\rho$. However, the induced vortex potentials close to the primary vortex core are very sensitive to the impurity concentration and momentum exchange during the tunneling process.

For a clean bulk SC, the Green's function can be parameterized similarly to (28) with $f \rightarrow f_S$, $\zeta \rightarrow \zeta_S$, and $\theta \rightarrow \theta_S$. The Eilenberger equations have the form of Eqs. (29) with $v_{2F} \rightarrow v_{||} = V_F \cos \chi_p$, where χ_p is the polar angle of the momentum, while $\Sigma_1 = 0$, $\Sigma_2 \rightarrow \Delta = \Delta_0(\rho)e^{i\phi}$, and $\Sigma_2^\dagger \rightarrow \Delta^*$. For energies $\epsilon \ll \Delta_\infty$ and distances s of the order of or less than the core size, the functions g_S and f_S are given in Refs. [27, 32], and

$$\zeta_S = \frac{\hbar v_{||} e^{-K}}{2\Lambda [\epsilon - \epsilon_0 \pm i\delta]},$$

$$\theta_S = \frac{2}{\hbar v_{||}} \int_0^s \left(\epsilon - \frac{b\Delta_0}{\rho'} \right) \zeta_S ds', \quad (31)$$

$$\epsilon_0(b) = \frac{b}{\Lambda} \int_0^\infty \frac{\Delta_0}{\rho} e^{-K(s)} ds, \quad (32)$$

$$\Lambda = \int_0^\infty e^{-K(s)} ds, \quad K(s) = \frac{2}{\hbar v_{||}} \int_{|b|}^\rho \Delta_0(\rho') d\rho'. \quad (33)$$

For larger distances $s \gg \xi_S$, the function ζ_S assumes its asymptotic expression $\zeta_S^{R(A)} = -b/\rho$ corresponding to the boundary conditions in Eq. (25).

3.1. Vortex potentials for coherent tunneling

The vortex potentials induced in the 2D layer crucially depend on the tunneling mechanism. For example, within the coherent tunneling model, we obtain

$$\Sigma_1 = i\Gamma g_S(\mathbf{Q}, \mathbf{r}), \Sigma_2 = i\Gamma f_S(\mathbf{Q}, \mathbf{r})$$

in terms of the infinite-space Green's functions, since $\check{g}_S(+Q_{3z}) = \check{g}_S(-Q_{3z})$ for specular reflection. For energies $\epsilon \ll \Delta_\infty$ and distances s of the order of or less than the core size ξ_S , it follows from Eq. (28) that

$$\begin{aligned} \Sigma_1 &= -\Gamma \zeta_S, \\ \Sigma_2 &= \Gamma [\theta_S - i\zeta_S] e^{i\alpha}, \\ \Sigma_2^\dagger &= \Gamma [\theta_S + i\zeta_S] e^{-i\alpha}, \end{aligned} \quad (34)$$

where ζ_S and θ_S are given by Eqs. (31)–(33).

3.2. Vortex potentials for incoherent tunneling

For incoherent tunneling, we find $\Sigma_1 = i\Gamma \langle g_S \rangle$, $\Sigma_2 = i\Gamma \langle f_S \rangle$, where averaging over the 3D momentum direction is equivalent to the ensemble averaging. To calculate the angular average, we can separate the Green's functions into the principal-value part and the delta-functional contribution. For example,

$$g_S^{R(A)} = i\zeta_S^{R(A)} = \text{V.P.} \left(\frac{i\hbar v_{||} e^{-K}}{2\Lambda (\epsilon - \epsilon_0)} \right) \pm \frac{\pi \hbar v_{||} e^{-K}}{2\Lambda} \delta(\epsilon - \epsilon_0). \quad (35)$$

Performing averaging over the polar χ_p and azimuthal α angles, we take the symmetry of the functions under the s -inversion transformation into account. As a result, we obtain

$$\Sigma_1 = -\Gamma \langle \zeta_S(s) \rangle, \quad (36)$$

$$\Sigma_2 e^{-i\phi} = \Sigma_2^\dagger e^{i\phi} = \Sigma_{ad} + \Sigma_2^{loc}, \quad (37)$$

$$\Sigma_{ad}(\rho) = \text{V.P.} \langle \Gamma I(s) \text{sign}(s) / 2\Lambda [\epsilon - \epsilon_0] \rangle, \quad (38)$$

where we set

$$I(s) = 2 \int_0^s \left(\epsilon - \frac{\Delta_0 b}{\rho} \right) e^{-K(s')} ds'.$$

The off-diagonal components of the induced potential are split into the localized and the long-range parts, Σ_2^{loc} and Σ_{ad} . The long-range function Σ_{ad} can be regarded as an adiabatic induced superconducting gap, $\Sigma_{ad} \rightarrow \Gamma$ for $\rho \gg \xi_S$ and $\Sigma_{ad} \rightarrow 0$ for $\rho \rightarrow 0$. Averaging over the azimuthal trajectory angle α , we find

$$\text{Re} \Sigma_2^{loc} = \Gamma \left\langle \frac{\hbar v_{||} e^{-K}}{2\Lambda \Omega \rho} \left[1 - \text{Re} \frac{|\epsilon|}{\sqrt{\epsilon^2 - \Omega^2 \rho^2}} \right] \right\rangle_z,$$

$$\text{Im} \Sigma_2^{loc} = \pm \Gamma \left\langle \text{Re} \frac{\epsilon \hbar v_{||} e^{-K}}{2\Lambda \Omega \rho \sqrt{\Omega^2 \rho^2 - \epsilon^2}} \right\rangle_z,$$

$$\text{Re} \Sigma_1 = -\text{sign}(\epsilon) \Gamma \left\langle \text{Re} \frac{\hbar v_{||} e^{-K}}{2\Lambda \sqrt{\epsilon^2 - \Omega^2 \rho^2}} \right\rangle_z,$$

$$\text{Im} \Sigma_1 = \pm \Gamma \left\langle \text{Re} \frac{\hbar v_{||} e^{-K}}{2\Lambda \sqrt{\Omega^2 \rho^2 - \epsilon^2}} \right\rangle_z,$$

where the upper (lower) sign corresponds to a retarded (advanced) self-energy term, $\Omega = d\epsilon_0/db$, and we use the notation

$$\langle \dots \rangle_z = \frac{1}{2} \int_0^\pi (\dots) \sin \chi_p d\chi_p$$

for the average over the polar angle χ_p of the 3D Fermi momentum. We note that our calculations are based on the first-order approximation in the small parameter b/ρ . According to Eq. (30), the symmetric $\Sigma_I(-s) = \Sigma_I(s)$ and antisymmetric $\Sigma_R(-s) = -\Sigma_R(s)$ parts of the off-diagonal self-energy term $\Sigma_2 e^{-i\phi}$ can be rewritten as $\Sigma_R = \Sigma_2 e^{-i\phi} s/\rho$ and $\Sigma_I = \Sigma_2 e^{-i\phi} b/\rho$.

The self-energy obtained above affects the vortex core states in the 2D layer in two different ways. The adiabatic part of the induced vortex potential leads to the Andreev localization of QPs with the energy smaller than the induced superconducting gap Γ within the induced vortex core at distances of the order of ξ_{2D} . This forms the CdGM anomalous branch $\epsilon_2(b)$ as in an usual SC with the corresponding maximum intrinsic gap Γ . Another part of the self-energy exponentially decaying at $\rho \sim \xi_S$ contains information about the CdGM states in the bulk SC; it affects the 2D-layer QP behavior at small scales. The adiabatic large-scale part of the self-energy (at $\rho \gg \xi_S$) is universal; it does not depend on the tunneling models and on possible disorder in the bulk SC, while the short-scale induced vortex potential localized at small distances does crucially depend on these factors. Both terms in the induced self-energy form the two-scale LDOS radial profile.

4. SCALE SEPARATION METHOD

A natural way to solve Eqs. (29) is to apply the scale separation method. We introduce a distance ρ_0 satisfying $\xi_S \ll \rho_0 \ll \xi_{2D}$ and consider the Green's functions in two overlapping spatial intervals, $\rho \lesssim \rho_0$ and $\rho \gtrsim \rho_0$. Next, we match the solutions in different spatial domains.

4.1. Large distances

At low energies $\epsilon \ll \Delta_\infty$ and large distances $\rho \gg \xi_S$, the induced vortex potential is given by Eq. (25). Quasiparticles propagating along the trajectories with impact parameters $b > \xi_S$ that miss the primary vortex core are affected only by this long-distance ($\xi_{2D} \gg \xi_S$) part of the induced gap potential. In the low-energy limit $\epsilon < \Gamma \ll \Delta_\infty$, the appropriate boundary conditions far from the induced vortex core ($\rho \gg \xi_{2D}$) are

$$\theta = \frac{\Gamma s/\rho}{\sqrt{\Gamma^2 - \epsilon^2}}, \quad \zeta = \frac{-\Gamma b/\rho}{\sqrt{\Gamma^2 - \epsilon^2}}, \quad g = \frac{-i\epsilon}{\sqrt{\Gamma^2 - \epsilon^2}}. \quad (39)$$

For both tunneling models and an arbitrary disorder rate inside the superconductor and for $\rho \gg \xi_S$, Eqs. (29) take the form

$$\begin{aligned} \hbar v_{2F} \frac{d\zeta}{ds} + 2\epsilon\theta - 2ig\Gamma s/\rho &= 0, \\ \hbar v_{2F} \frac{d\theta}{ds} - 2\epsilon\zeta - 2ig\Gamma b/\rho &= 0, \\ \hbar v_{2F} \frac{dg}{ds} + 2i\theta\Gamma b/\rho + 2i\zeta\Gamma s/\rho &= 0. \end{aligned} \quad (40)$$

The functions g and ζ are even in s while θ is odd, and we can therefore consider only positive s values. We obtain the solution of the above equations using the first-order perturbation theory in the impact parameter b : $\check{w}(s) = \check{w}_0(s) + \check{w}_1(s)$, where $\check{w}(s) = (\zeta, \theta, ig)^T$. As we see in what follows, this approximation holds for $|b| \ll \xi_{2D}$. The zeroth order in the b solution is given by

$$\check{w}_0(s) = \frac{1}{\sqrt{\Gamma^2 - \epsilon^2}} \check{u}_0(s) + \frac{C}{\sqrt{\Gamma^2 - \epsilon^2}} \check{u}_-(s), \quad (41)$$

where

$$\check{u}_\pm(s) = \begin{pmatrix} \sqrt{\Gamma^2 - \epsilon^2} \\ \pm\epsilon \\ \pm\Gamma \end{pmatrix} e^{\pm\lambda s}, \quad \check{u}_0(s) = \begin{pmatrix} 0 \\ \Gamma \\ \epsilon \end{pmatrix},$$

and $\lambda = 2\sqrt{\Gamma^2 - \epsilon^2}/\hbar v_{2F}$. This solution satisfies the boundary conditions $g = -i\epsilon/\sqrt{\Gamma^2 - \epsilon^2}$, $\zeta = 0$, and $\theta = \Gamma/\sqrt{\Gamma^2 - \epsilon^2}$ for $s \rightarrow \infty$ and $\epsilon^2 < \Gamma^2$. The first-order correction \check{w}_1 can be written as

$$\check{w}_1(s) = \frac{C_0(s)\check{u}_0}{\sqrt{\Gamma^2 - \epsilon^2}} + \frac{C_+(s)\check{u}_+}{\sqrt{\Gamma^2 - \epsilon^2}} + \frac{C_-(s)\check{u}_-}{\sqrt{\Gamma^2 - \epsilon^2}}, \quad (42)$$

where

$$\begin{aligned} \xi_{2D} C_0(s) &= 2Cb \int_s^\infty e^{-\lambda s} \frac{ds}{\rho}, \\ \xi_{2D} C_+(s) &= -b \int_s^\infty e^{-\lambda s} \frac{ds}{\rho}, \\ \xi_{2D} C_-(s) &= -b \int_{s_c}^s e^{\lambda s} \frac{ds}{\rho}. \end{aligned} \quad (43)$$

The lower limit of integration in C_- , s_c , has to be taken as $s_c \sim \xi_S$ for trajectories that go through the primary vortex core, $b \lesssim \xi_S$, such that the logarithmic divergence be cut off at the distances of the order of ξ_S , where the long-range vortex potential Σ_{ad} in (38) vanishes. For $b \gg \xi_S$, we have $s_c = 0$. The perturbation approach holds as long as $C_0 \ll C$ and $C_+ \ll 1$, i. e., as long as $|b| \ll \xi_{2D}$. For $s \gg \xi_{2D}$, the coefficient C_0 decays faster than exponentially, while

$$C_+(s)e^{\lambda s} \rightarrow C_-(s)e^{-\lambda s} \rightarrow -\frac{\Gamma}{2\sqrt{\Gamma^2 - \epsilon^2}} \frac{b}{\rho}$$

and hence ζ approaches $-(b/\rho)\Gamma/\sqrt{\Gamma^2 - \epsilon^2}$ and the corrections to θ and g vanish, as they should in accordance with (39). For a small distance $s = s_0$ defined as $\rho_0^2 = s_0^2 + b^2$, we have

$$\zeta(s_0) = C + C_+(s_0) + C_-(s_0), \quad (44a)$$

$$\theta(s_0) = \frac{1}{\sqrt{\Gamma^2 - \epsilon^2}} \{ \Gamma - \epsilon C + \Gamma C_0(s_0) + \epsilon [C_+(s_0) - C_-(s_0)] \}, \quad (44b)$$

$$g(s_0) = \frac{i}{\sqrt{\Gamma^2 - \epsilon^2}} \{ -\epsilon + \Gamma C - \epsilon C_0(s_0) - \Gamma [C_+(s_0) - C_-(s_0)] \}. \quad (44c)$$

4.2. Matching for large impact parameters

Far from the primary vortex core at impact parameters $\xi_S \ll b \ll \xi_{2D}$, the perturbative result in Eqs. (40) can be applied along the entire trajectory, and we can therefore set $s_0 = s_c = 0$. The boundary condition for an odd function requires $\theta(0) = 0$. Because $C_-(0) = 0$ in this case, we find from Eq. (44b) that

$$\Gamma + \epsilon C_+(0) = \epsilon C - \Gamma C_0(0).$$

Expressing the coefficients C_0 and C_+ in terms of the energy

$$\epsilon = \epsilon_2(b) = \frac{2\Gamma^2 b}{\hbar v_{2F}} \ln \eta \quad (45)$$

of bound states in the induced vortex core, with $\eta = \xi_{2D}/|b|$ and $C_0 = -2CC_+ = C\epsilon_2(b)/\Gamma$, we find

$$C[\epsilon - \epsilon_2(b)] = \Gamma - \epsilon\epsilon_2(b)/2\Gamma. \quad (46)$$

According to Eq. (46), $\epsilon_2(b)$ is the only spectrum branch in the energy interval $|\epsilon| \ll \Delta_\infty$. The Green's function is

$$g(s) = \frac{-i\epsilon}{\sqrt{\Gamma^2 - \epsilon^2}} + \frac{i\Gamma C}{\sqrt{\Gamma^2 - \epsilon^2}} e^{-\lambda s} - \frac{i\epsilon C_0(s)}{\sqrt{\Gamma^2 - \epsilon^2}} - \frac{i\Gamma}{\sqrt{\Gamma^2 - \epsilon^2}} [C_+(s)e^{\lambda s} - C_-(s)e^{-\lambda s}]. \quad (47)$$

For $s \gg \xi_{2D}$, we have $C_0 \rightarrow 0$ and $C_+ e^{\lambda s} - C_- e^{-\lambda s} \rightarrow 0$, whence it follows that the first term is the homogeneous background while the rest terms describe the vortex contribution. To obtain the retarded function for $\epsilon^2 > \Gamma^2$, we have to continue $\sqrt{\Gamma^2 - \epsilon^2}$ analytically to the upper half-plane of complex ϵ keeping $\text{Re} \sqrt{\Gamma^2 - \epsilon^2} > 0$.

4.3. Matching for small impact parameters

To find the Green's functions for small impact parameters $b \lesssim \xi_S$, we have to match Eqs. (44) with the solution obtained in the vortex core region. For small $s < s_0$, we assume that the even parts of the Green's functions $g(s)$ and $\zeta(s)$ are nearly constant in the interval $0 < s < s_0$. Integrating Eq. (29b) over s from 0 to s_0 along the trajectory, we find the matching condition

$$\frac{\hbar v_{2F}}{2} \theta(s_0) = \zeta(s_0) \int_0^{s_0} \Sigma_1 ds + ig(s_0) \int_0^{s_0} \Sigma_I ds. \quad (48)$$

Equation (48) determines the constant C . Its poles define the eigenstates of excitations as functions of energy and the impact parameter. In deriving the effective boundary condition (48) for $b \lesssim \xi_S$, we need to separate the exponentially converging parts $\Sigma_{1,I}^{loc}$ at $s \sim \xi_S$ from the long-distance ($s \gg \xi_S$) asymptotics of $\Sigma_{1,I}$. For $\epsilon \ll \Delta_\infty$, long-distance expressions (25) yield $\Sigma_1 \rightarrow 0$ and $\Sigma_I \rightarrow \Gamma b/\rho$. Therefore,

$$\begin{aligned} \int_0^{s_0} \Sigma_I ds &= \int_0^{\xi_S} \Sigma_I^{loc} ds + \Gamma \int_{\xi_S}^{s_0} \frac{b}{\rho} ds \approx \\ &\approx \int_0^\infty \Sigma_I^{loc} ds + \Gamma b \ln \frac{s_0}{\xi_S}, \end{aligned} \quad (49)$$

while $\int_0^{s_0} \Sigma_1 ds$ can be extended to infinity. The localized self-energy parts Σ_1 and Σ_I^{loc} determine the small-distance LDOS and the spectrum of excitations and depend on the particular tunneling mechanism.

5. MULTIPLE VORTEX CORE IN THE CLEAN LIMIT. QUASIPARTICLE SPECTRUM AND DENSITY OF STATES

5.1. Isotropic Fermi surface

In this section, we consider an idealized picture without any disorder. For large impact parameters $b \gg \xi_S$, the corresponding solutions for the Green's functions, Eq. (47), coincide with the standard CdGM expressions where the gap value is replaced with Γ . The corresponding anomalous spectrum for 2D excitations is given by Eq. (45) [27, 32]. This modified CdGM branch dominates in the LDOS at large distances $\rho \gg \xi_S$.

The normalized LDOS is defined as an average over the trajectories:

$$N(\mathbf{r}, \epsilon) = \int_0^{2\pi} N_\epsilon(s, b) \frac{d\alpha'}{2\pi} = \int_{-\rho}^{\rho} \frac{N_\epsilon(\sqrt{\rho^2 - b^2}, b) db}{\sqrt{\rho^2 - b^2} \pi},$$

where

$$N_\epsilon(s, b) = [g^R(s, b) - g^A(s, b)] / 2, \\ s = \rho \cos \alpha', \quad b = -\rho \sin \alpha'.$$

For $|\epsilon| < \Gamma$, a nonzero LDOS comes only from the vortex contribution of the second and third terms in (47) due to the presence of a pole in the coefficient C according to Eq. (46). The Green's functions and LDOS reach their long-distance values $g = -i\epsilon/\sqrt{\Gamma^2 - \epsilon^2}$ and $N = \text{Re} |\epsilon|/\sqrt{\epsilon^2 - \Gamma^2}$ as $\rho \rightarrow \infty$. For $\rho \gg \xi_S$, the trajectories with large impact parameters $b \gtrsim \xi_S$ give the main contribution to the LDOS. In the region $\xi_S \ll \rho \ll \xi_{2D}$, we obtain the angle-resolved DOS in the form

$$N_\epsilon(s, b) = \frac{\sqrt{\Gamma^2 - \epsilon^2}(\Gamma^2 - \epsilon^2/2)}{\Gamma^2} \times \\ \times \pi \delta[\epsilon - \epsilon_2(b)], \quad |\epsilon| < \Gamma, \quad (50)$$

$$N_\epsilon(s, b) = \frac{\sqrt{\epsilon^2 - \Gamma^2}[\Gamma^2 - \epsilon_2^2(b)/2]}{\text{sign}(\epsilon)\Gamma^2[\epsilon - \epsilon_2(b)]}, \quad |\epsilon| > \Gamma. \quad (51)$$

Hence, the corresponding LDOS in the energy interval $|\epsilon| < \Gamma$ has the only peaks at $\epsilon = \epsilon_2(\pm\rho)$:

$$N(\rho, \epsilon) = \frac{1}{\pi} \int_{-\rho}^{\rho} N_\epsilon(\sqrt{\rho^2 - b^2}, b) \frac{db}{\sqrt{\rho^2 - b^2}} = \\ = \text{Re} \frac{\sqrt{\Gamma^2 - \epsilon^2}(1 - \epsilon^2/2\Gamma^2)}{\sqrt{\epsilon_2^2(\rho) - \epsilon^2}}. \quad (52)$$

For energies above the induced gap, $|\epsilon| > \Gamma$, for the same distances, the LDOS monotonically increases with $|\epsilon|$ to its normal-state value:

$$N(\rho, \epsilon) = \sqrt{\epsilon^2 - \Gamma^2} \left[\frac{|\epsilon|}{2\Gamma^2} + \frac{(1 - \epsilon^2/2\Gamma^2)}{\sqrt{\epsilon^2 - \epsilon_2^2(\rho)}} \right]. \quad (53)$$

A trajectory with a small impact parameter $b \lesssim \xi_S$ can be divided into the part far from the primary vortex core and the region inside the core. Far from the core, the solution is found using vortex potentials (25). The self-energies of the primary vortex in Eq. (18) have poles at the usual CdGM energy $\epsilon_0(b)$ with the corresponding wave functions exponentially localized within

$\rho \sim \xi_S$ and the regular parts extending over large distances $\rho \rightarrow \pm\infty$ [27, 32]:

$$\Sigma_R = \Gamma\theta_S, \quad \Sigma_I = -\Gamma\zeta_S. \quad (54)$$

We note that the localized part Σ_2^{loc} of the effective order parameter Σ_2 has the coordinate dependence $\Sigma_2^{loc} = i\Sigma_I^{loc}(b, s)e^{i\alpha}$ with zero circulation, unlike its adiabatic part (25), $\Sigma_2(\rho \gg \xi_S) = \Gamma e^{i\phi}$. As we see below, it is this different angular dependence of the effective gap asymptotics, which leads to the formation of a ‘‘shadow’’ of the bulk SC anomalous branch in the excitation spectrum and LDOS in the 2D layer.

Using Eqs. (43) for the long-distance part of the trajectory, we find

$$C_0(s_0) = \frac{2Cb}{\xi_{2D}} \ln \frac{1}{\lambda s_0}, \\ C_+(s_0) \pm C_-(s_0) \approx -\frac{b}{\xi_{2D}} \ln \frac{1}{\lambda \xi_S} \approx -\frac{\epsilon_2(b)}{2\Gamma}. \quad (55)$$

We now match asymptotic solution (44) obtained for $s \geq s_0$ with the solution for the short-distance part of the trajectory in Eqs. (34) and (31)–(33), using Eq. (48) and Eq. (49). As a result,

$$C \left\{ \xi_{2D} [\epsilon - \epsilon_2(b)] + 2 \left[\Gamma - \sqrt{\Gamma^2 - \epsilon^2} - \frac{\epsilon\epsilon_2(b)}{\Gamma} \right] \times \right. \\ \left. \times \int_0^\infty \zeta_0 ds \right\} = \xi_{2D}\Gamma + 2\epsilon \int_0^\infty \zeta_0 ds - \xi_{2D} \frac{\epsilon\epsilon_2(b)}{2\Gamma} - \\ - \left(\Gamma + \sqrt{\Gamma^2 - \epsilon^2} \right) \frac{\epsilon_2(b)}{\Gamma} \int_0^\infty \zeta_0 ds, \quad (56)$$

where $\zeta_0(s)$ is the localized part of ζ_S and

$$\int_0^\infty \zeta_0 ds = \frac{\hbar v_\parallel}{2[\epsilon - \epsilon_0(b)]}. \quad (57)$$

Here, we put $g = i\zeta_0$ and replace the cutoff parameter in (45) with $\eta = \xi_{2D}/\xi_S$. For $b \gg \xi_S$, the contributions from the primary vortex core proportional to $\int_0^\infty \zeta_0 ds$ vanish since the trajectory misses the core, and Eq. (56) goes over into Eq. (46).

For small $b \ll \xi_{2D}$, the Green's function has a pole when

$$P(\epsilon, b) = [\epsilon - \epsilon_2(b)][\epsilon - \epsilon_0(b)] + \\ + q_v \left[\Gamma^2 - \Gamma\sqrt{\Gamma^2 - \epsilon^2} - \epsilon\epsilon_2(b) \right] = 0, \quad (58)$$

where $q_v = v_\parallel/v_{2F}$. It can be shown that with the higher-order terms in the parameter $\epsilon_2(b)/\Gamma$ included,

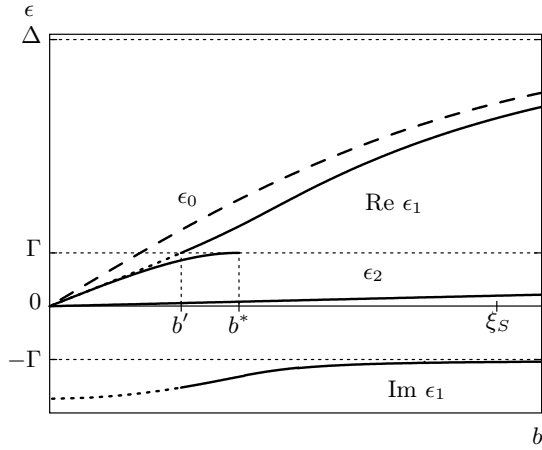


Fig. 5. Two localized branches, $\epsilon_1(b)$ and $\epsilon_2(b)$, of the spectrum in Eq. (59), in the limit of coherent tunneling, for $\epsilon < \Gamma$. Here, b^* is defined as $\epsilon_1(b^*) = \Gamma - 0$, and b' corresponds to $\text{Re } \epsilon_1(b') = \Gamma + 0$. The spectrum satisfies $\epsilon_{1,2}(-b) = -\epsilon_{1,2}^*(b)$

the corresponding energy dispersion relation takes the form

$$\frac{[\epsilon - \epsilon_2(b)][\epsilon - \epsilon_0(b)]}{\Gamma q_v} + \Gamma - \sqrt{\Gamma^2 - [\epsilon - \epsilon_2(b)]^2} = 0. \quad (59)$$

For $b \lesssim \xi_S$, the cutoff parameter in Eq. (45) should be replaced with $\eta = \xi_{2D}/\xi_S$.

The resulting two-scale spectrum is shown in Fig. 5. There are two real-valued branches in the range $|\epsilon| < \Gamma$ crossing zero energy value as functions of the impact parameter and one complex-valued branch in the range $\Gamma < |\epsilon| < \Delta_\infty$. The lowest-energy branch $\epsilon_2(b)$ has a scale ξ_{2D} as a function of the impact parameter: for $b \lesssim \xi_{2D}$, it is given by Eq. (45) with the proper cutoff parameter η as discussed above and saturates at $\epsilon = \Gamma$ for $b \gg \xi_{2D}$. The branch $\epsilon_1(b)$ has a scale ξ_S : for $\epsilon < \Gamma$ it goes slightly below the CdGM spectrum $\epsilon_0(b)$ of the bulk SC, $\epsilon_1(b) = (1 + q_v/2)^{-1}\epsilon_0(b)$. Above Γ , the spectrum transforms into a scattering resonance due to the decay into delocalized modes propagating in the 2D layer: $\epsilon_1(b) = \epsilon_0(b) - i\Gamma q_v$ for $|\epsilon| \gg \Gamma$. Since Eq. (59) determines a pole of the retarded Green's function in the lower half-plane of complex ϵ , the square root in Eq. (59) should be analytically continued through the cut going from $-\infty$ to $-\Gamma$ and from Γ to $+\infty$. As a result, $\epsilon_1(b)$ has a discontinuity at $\epsilon_1 = \Gamma$ with $b'/\xi_S \approx 0.29$ and $b^*/\xi_S \approx 0.42$.

The two branches appear due to the presence of two sub-systems, the bulk SC and the 2D proximity layer, each with its own anomalous branch. The existence of two anomalous branches follows also from the index

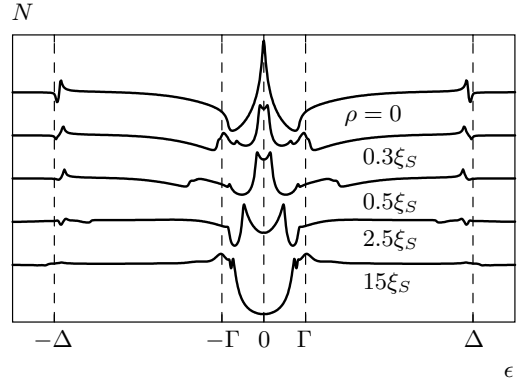


Fig. 6. LDOS in a logarithmic scale for coherent tunneling in the clean limit. The curves, taken for different distances ρ from the vortex center, are vertically shifted for clarity. The peaks in the LDOS exist up to distances $\sim \xi_{2D}$. Here, $\Delta/\Gamma = 5$ and $q_v = 1$

theorem [33, 34]. Indeed, its application requires that both zero of the QC Hamiltonian at the Fermi surface and its singularity at $\epsilon = \epsilon_0(b)$ be taken into account in calculating the topological invariant. As a result, the number of anomalous branches increases to 2 for a single-quantum vortex.

The multiple-branch spectrum results in a multiple-peak structure in the LDOS (Fig. 6), which appears to be most pronounced deeply inside the primary core (at distances $\rho \lesssim \xi_S^2/\xi_{2D}$ when $\epsilon_1 < \Gamma$), thus illustrating the two-scale structure of the vortex core. The LDOS is obtained from the angle-resolved DOS (normalized by its normal state value) $N_\epsilon(s, b) = [g^R(s, b) - g^A(s, b)]/2$ averaged over the trajectory direction.

The angle-resolved DOS for small energies $|\epsilon| \ll \Gamma$ and $\rho \lesssim \xi_S$ is given by

$$N_\epsilon(s, b) = \frac{1}{2}\pi\Gamma q_v \delta[\epsilon - \epsilon_1(b)] + \frac{1}{2}\pi\Gamma(q_v + 2)\delta[\epsilon - \epsilon_2(b)], \quad (60)$$

where we neglect the terms $\epsilon\epsilon_2(b)/\Gamma^2$ and $\epsilon_2(b)/\epsilon_1(b)$ and put $\epsilon_0(b)/\epsilon_1(b) = 1 + q_v/2$ according to low-energy asymptotics. In this case, the LDOS

$$N(\rho, \epsilon) = \text{Re} \frac{\Gamma q_v}{2\sqrt{\epsilon_1^2(\rho) - \epsilon^2}} + \text{Re} \frac{\Gamma(q_v + 2)}{2\sqrt{\epsilon_2^2(\rho) - \epsilon^2}} \quad (61)$$

reveals a two-peak structure vs energy at $\epsilon = \epsilon_{1,2}(\rho)$. For $|\epsilon| \sim \Gamma$, we can neglect $\epsilon_2(b)$ and obtain

$$[\epsilon - \epsilon_0(b)] \left[\Gamma + \sqrt{\Gamma^2 - \epsilon^2} \right] + q_v \Gamma \epsilon = 0. \quad (62)$$

For $|\epsilon| > \Gamma$, the dispersion relation is complex-valued and for the retarded functions takes the form

$$\epsilon[\epsilon - \epsilon_0(b)] + q_v \Gamma \left[\Gamma + i \operatorname{sign}(\epsilon) \sqrt{\epsilon^2 - \Gamma^2} \right] = 0. \quad (63)$$

The last equation describes the resonant states in the 2D vortex core that decay into the QP waves propagating in the 2D layer above the induced gap.

Finally, the whole spectrum structure, shown in Fig. 5, has two anomalous branches: one of them, $\epsilon_2(b)$, is completely real-valued and follows the CdGM spectrum for the superconductor with a homogeneous gap Γ ; the other one is close to the bulk CdGM spectrum, but has a discontinuity at $\epsilon = \Gamma$, where it becomes essentially complex.

Thus, the LDOS for energies above the induced gap $|\epsilon| > \Gamma$ and small distances $\rho, b \lesssim \xi_S$ is given by

$$N(\rho, \epsilon) = \frac{\sqrt{\epsilon^2 - \Gamma^2}}{|\epsilon|} + \frac{q_v \Gamma^2}{2|\epsilon|} \times \operatorname{Re} \frac{\sqrt{\epsilon^2 - \Gamma^2} - i\Gamma}{\sqrt{(\epsilon^2 + q_v \Gamma^2 + i q_v \Gamma \sqrt{\epsilon^2 - \Gamma^2})^2 - \epsilon^2 \epsilon_0^2(\rho)}} \quad (64)$$

and has the only peak at $\epsilon = \operatorname{Re} \epsilon_1(\rho)$ of the height $\sim \Gamma^2/\epsilon_0^2(\rho)$ for $\rho \gtrsim \xi_S^2/\xi_{2D}$. In the opposite limit of rather large distances $\rho > \xi_S^2/\xi_{2D}$ at $|\epsilon| > \Gamma$, the spectrum reduces to the CdGM spectrum with a finite broadening:

$$\epsilon_1(b) = \epsilon_0(b) - i\Gamma q_v. \quad (65)$$

The LDOS has a small difference from its normal-state value $N_0 = 1$:

$$N(\rho, \epsilon) = 1 + \frac{q_v \Gamma^2}{2\epsilon^2} \operatorname{Re} \frac{|\epsilon| - i\Gamma}{\sqrt{(\epsilon + i q_v \Gamma)^2 - \epsilon_0^2(\rho)}}. \quad (66)$$

The LDOS in the whole energy range, Eqs. (61) and (64), has two or even three peaks for such distances. The latter case is realized at the distances corresponding to $b' < b < b^*$, where the spectrum vs the impact parameter has three anomalous branches.

The numerical LDOS patterns have been obtained by subsequently solving the two sets of Eilenberger equations in the Riccati parameterization [35]: first, we calculate the Green's functions in the bulk SC using the approximation $\Delta_0(\rho) = \Delta_\infty \rho / \sqrt{\rho^2 + \xi_S^2}$ and next we solve Eq. (18) in the 2D layer using Eq. (19).

5.2. Anisotropic Fermi surface

Here, we briefly discuss the effects of anisotropic Fermi surfaces in 3D and/or 2D systems. We are interested only in main distinctions that the anisotropy

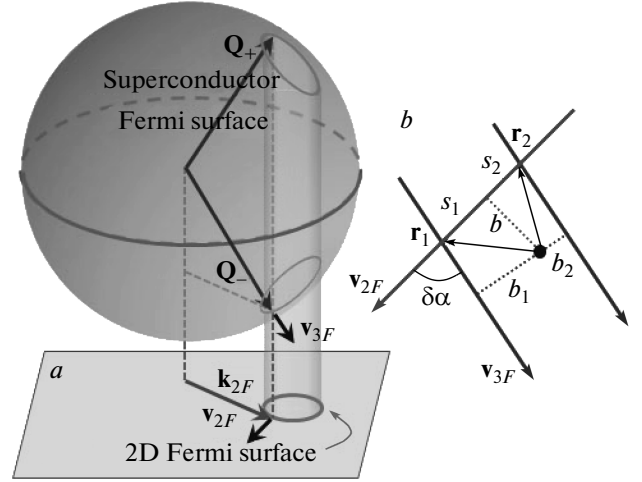


Fig. 7. (a) An example of anisotropic Fermi surfaces showing a spherical 3D Fermi surface showing a spherical 3D Fermi surface on top of a part of a 2D Fermi surface in the layer shifted from the center of its Brillouin zone. The closed loops show the 2D Fermi line and its projections onto the 3D Fermi surface. The directions of the 3D Fermi velocity projection \mathbf{v}_{3F} on the plane $z = 0$ in the bulk does not coincide with that in the 2D layer, \mathbf{v}_{2F} . (b) Different points \mathbf{r}_1 and \mathbf{r}_2 specified by s_1 and s_2 on a 2D trajectory with a given impact parameter b belong to trajectories in 3D with different impact parameters b_1 and b_2

causes within the coherent tunneling model as compared to the isotropic case considered above. For anisotropic surfaces, one can also apply the method of scale separation in the same manner as we did in Sec. 4. The consideration for the region of large impact parameters does not differ significantly, such that the solution for the Green's functions together with the matching conditions look similar to Eqs. (41), (43), (55) and (48), (49). But the region of small impact parameters of the order of ξ_S gives an essentially different result. The main distinction is that the directions of QP trajectories determined by the group velocities $\partial \epsilon_{2D} / \partial \mathbf{k}$ and $\partial \epsilon_{3D} / \partial \mathbf{Q}$ for a given in-plane momentum in 2D and 3D systems do not coincide (Fig. 7a). As a result, the integral in Eq. (48) along a 2D trajectory involves trajectories with different impact parameters used to parameterize the 3D Green's functions (Fig. 7b). Within the QC approximation, the integral then yields an imaginary part that comes from the delta function at the 3D core spectrum and a real contribution from a smooth dependence. The spectrum $\epsilon_2(b)$ at small impact parameters thus becomes broadened and shifted from its initial position. The imaginary contribution appears due to the coupling of the

QC trajectory in the 2D layer with a QC continuum of trajectories inside the superconductor corresponding to different impact parameters. This coupling results from the nonconservation of the angular momentum in the anisotropic system. The imaginary contribution is also present if the primary-core spectrum is broadened by disorder or inelastic scattering. The situation is in many respects similar to that in the incoherent tunneling model discussed in the next section. Of course, attributing the origin of the imaginary part of energy in the anisotropic case to the continuum of states in the bulk SC, we ignore the angular momentum quantization in the primary vortex core. The true quantum-mechanical consideration accounting for the level quantization could possibly change this conclusion and lead to a real-valued energy spectrum for ideal systems without disorder.

In this section, we consider the low-energy behavior of the Green's function at small impact parameters $b \ll \xi_S$, where the spectral energy $\epsilon_2(b)$ is very small and can be neglected. We assume that the trajectories in the bulk SC and in the 2D layer do not coincide; the Fermi velocities \mathbf{v}_{2F} and \mathbf{v}_{3F} are at an angle $\delta\alpha$ to each other (see Fig. 7*b*). The impact parameter b_S and trajectory coordinate s_S in the superconductor are coupled to the ones in the 2D layer (b and s) via

$$b_S = \rho \sin(\phi - \alpha + \delta\alpha) = b \cos \delta\alpha + s \sin \delta\alpha,$$

$$s_S = \rho \cos(\phi - \alpha + \delta\alpha) = s \cos \delta\alpha - b \sin \delta\alpha.$$

As we know, at small distances $\rho \ll \xi_S$, the part ζ_S of the anomalous Green's function f_S in the bulk SC is large compared with $\zeta_S \gg \theta_S$. Neglecting the latter, we express the self-energies in Eq. (30) as

$$\Sigma_R = \Sigma_1 \sin \delta\alpha, \tag{67a}$$

$$\Sigma_I = \Sigma_1 \cos \delta\alpha. \tag{67b}$$

The diagonal self-energy is $\Sigma_1 = i\Gamma g_S \approx -\Gamma \zeta_S$. We note that the self-energies depend on the trajectory coordinate s in a 2D layer through the impact parameter $b_S = b \cos \delta\alpha + s \sin \delta\alpha$ in the bulk SC and do not have definite symmetry in s . Therefore, we need to consider the region inside the primary core more carefully, allowing for contributions from even and odd components of the corresponding functions.

As in Sec. 4, we use the scale separation method and subdivide a 2D layer trajectory with a small impact parameter $b \lesssim \xi_S$ into the long-distance part far from the primary vortex core and the region inside the core. We introduce a distance ρ' satisfying $\xi_S \ll \rho' \ll \xi_{2D}$ and consider the Green's functions in two overlapping

spatial intervals, $\rho \lesssim \rho'$ and $\rho \gtrsim \rho'$. Next, we match the solutions in different spatial domains. Far from the core, the solution is found using vortex potentials Eq. (25).

In the region inside the primary vortex core, the self-energies play the most important role. Using the approximation in (67) for the self-energies and neglecting ϵ at small distances $s < s_0$, we find

$$\zeta \cos \delta\alpha - \theta \sin \delta\alpha + ig = C_1$$

from Eqs. (29), where C_1 is a constant and

$$\frac{d}{ds} (\zeta \sin \delta\alpha + \theta \cos \delta\alpha) = \frac{2\Sigma_1}{\hbar v_{2F}} (\zeta \cos \delta\alpha - \theta \sin \delta\alpha + ig).$$

This equation yields

$$\zeta \sin \delta\alpha + \theta \cos \delta\alpha = C_1 \int_0^s \frac{2\Sigma_1(s')}{\hbar v_{2F}} ds' + C_2.$$

Eliminating the constants C_1 and C_2 , we find the following matching conditions at $s = \pm s_0$:

$$[\zeta \cos \delta\alpha - \theta \sin \delta\alpha + ig]_{s_0} = 0, \tag{68a}$$

$$[\zeta \sin \delta\alpha + \theta \cos \delta\alpha]_{s_0} + I_{odd} \{ \zeta \cos \delta\alpha - \theta \sin \delta\alpha + ig \}_{s_0} = 0, \tag{68b}$$

where $[x]_{s_0} = x(s_0) - x(-s_0)$, $\{x\}_{s_0} = x(s_0) + x(-s_0)$, and the integral

$$I_{odd} = \frac{\Gamma}{\hbar v_{2F}} \int_{-s_0}^{s_0} \zeta_S(s') ds'$$

takes the form

$$I_{odd} = \frac{\Gamma v_{\parallel}}{v_{2F} 2\Lambda \sin \delta\alpha} \times \\ \times \text{V.P.} \int_{-\infty}^{\infty} \frac{\exp[-K(z \text{ctg} \delta\alpha - b \sin \delta\alpha)]}{\epsilon - \epsilon_0(b \cos \delta\alpha + z)} dz \mp \\ \mp \frac{i\pi v_{\parallel} \Gamma}{2\Lambda v_{2F} \Omega \sin \delta\alpha} \times \\ \times \exp \left[-K \left(\frac{\epsilon \text{ctg} \delta\alpha}{\Omega} - \frac{b}{\sin \delta\alpha} \right) \right], \tag{69}$$

where we put $s \sin \delta\alpha = z$. The second term comes from the delta-function contribution at one of the primary core states (see Eq. (31)); the upper (lower) sign corresponds to the retarded (advanced) function. For $\delta\alpha \lesssim \epsilon/\Delta$, the second term disappears while the first

gives the real pole contribution, which is equivalent to Eq. (57). We conclude that the imaginary part disappears only for trajectories that are almost parallel (within an angle $\delta\alpha \lesssim \epsilon/\Delta$). For $\delta\alpha \gg \epsilon/\Delta$, the first (real) term vanishes because the integrand becomes odd in z . For $\epsilon = 0$ and $b = 0$, the real term vanishes exactly.

Equations (68) are the matching conditions with the solution in the large-distance region $s > s_0$. They are generalizations of the matching condition in Eq. (48) derived earlier in the isotropic situation. The two conditions in Eqs. (68) determine the even and odd parts of the Green's functions.

The long-distance solution is found in the same way as in Sec. 4. However, it no longer has a definite symmetry with respect to $s \rightarrow -s$. We separate the even and odd components $\check{w} = \check{w}_{even} + \check{w}_{odd}$ and consider both $s > 0$ and $s < 0$. In this section, we only discuss the behavior of the Green's function for low energies and a small impact parameter. We therefore neglect the corrections to \check{w} proportional to b/ξ_{2D} . In this case, \check{w}_{even} is given by Eq. (41), where now

$$\check{u}_{\pm}(s) = \begin{pmatrix} \sqrt{\Gamma^2 - \epsilon^2} \\ \pm\epsilon \operatorname{sign} s \\ \pm\Gamma \end{pmatrix} e^{\pm\lambda|s|}, \quad \check{u}_0(s) = \begin{pmatrix} 0 \\ \Gamma \operatorname{sign} s \\ \epsilon \end{pmatrix}$$

and

$$\check{w}_{odd} = \frac{\tilde{C} \operatorname{sign} s}{\sqrt{\Gamma^2 - \epsilon^2}} \check{u}_-(s). \quad (70)$$

Equation (68a) gives

$$\tilde{C} = \frac{\sin \delta\alpha (\Gamma - C\epsilon)}{\sqrt{\Gamma^2 - \epsilon^2} \cos \delta\alpha - \Gamma}. \quad (71)$$

Using Eqs. (41), (70), and (71), we find the combinations $\zeta(s_0) \pm \zeta(-s_0)$, $\theta(s_0) \pm \theta(-s_0)$, and $ig(s_0) + ig(-s_0)$ in terms of the coefficient C . Next, we insert these combinations into Eq. (68b) and find

$$C[\epsilon - Y I_{odd}] = \Gamma + \epsilon I_{odd} \cos \delta\alpha, \quad (72)$$

where

$$Y = \sqrt{\Gamma^2 - \epsilon^2} - \Gamma \cos \delta\alpha. \quad (73)$$

Equations (72) and (73) are the counterparts of Eq. (46) for the asymmetric case and transform into Eq. (46) as $\delta\alpha \rightarrow 0$.

For $\epsilon \ll \Gamma$, we have $Y = \Gamma(1 - \cos \delta\alpha)$. For $\delta\alpha \gtrsim \epsilon/\Delta$, the integral I_{odd} in Eq. (69) has only the imaginary part. Therefore,

$$C = \frac{\Gamma}{\epsilon - \epsilon_2(b) \pm i\gamma}, \quad (74)$$

where

$$\gamma = \frac{\pi v_{\parallel} \Gamma^2 \operatorname{tg}(\delta\alpha/2)}{\Lambda v_{2F} \Omega} \exp[-K(\rho_0)] \sim \frac{\Gamma^2}{\Delta} \quad (75)$$

and $\rho_0 = |b/\sin \delta\alpha|$. In Eq. (74), we include the energy $\epsilon_2(b)$, which can be obtained by more detailed calculations taking the corrections due to b/ρ into account in the same way as in Sec. 4. The function $\exp[-K(\rho_0)]$ decays exponentially as $\exp(-\rho_0/\xi_S)$ for impact parameters larger than the primary core size, $b \gtrsim \xi_S$.

Therefore, the imaginary term in (74) does not disappear unless $\delta\alpha$ is very small. It results in a smearing of the adiabatic energy level $\epsilon_2(b) \ll \Gamma$ and in a Lorentzian behavior of the DOS due to tunneling into the primary vortex core states. We recall that this result is obtained within the QC approximation.

6. DISORDER EFFECTS

6.1. Multiple core. Clean limit with incoherent tunneling

We study the disorder effects by introducing the momentum scattering first into the tunneling process described by the incoherent tunneling model. Since the tunneling is considered as a perturbation, we can assume a specular QP scattering at the interface on the bulk side and, thus, use the results in the preceding section for the Green's functions. The self-energy potentials are now obtained by averaging the Green's functions (31)–(33) over the trajectory direction: $\check{\Sigma}_T = i\Gamma \langle \check{g}_S \rangle$. Of course, this averaging does not affect the induced gap function (25) outside the primary vortex core, and therefore the spectrum ϵ_2 survives the influence of the tunnel barrier disorder at least for $b > \xi_S$. On the contrary, the subgap branches localized within the primary vortex core are completely destroyed. This dramatic consequence of the momentum scattering is caused by the averaging of electron wave functions with different impact parameters and consequent loss of information about the CdGM states of the primary vortex. A natural consequence of the momentum scattering is the appearance of a finite broadening of energy levels for trajectories with small impact parameters $b \lesssim \xi_S$. Matching the solutions in the core and at large distances gives the expression for the coefficient C for $b \lesssim \xi_S$ and $|\epsilon| \ll \Gamma$:

$$C \left[\epsilon - \epsilon_2(b) + \frac{2\sqrt{\Gamma^2 - \epsilon^2}}{\hbar v_{2F}} \int_0^\infty \Sigma_1 ds - \frac{2\Gamma}{\hbar v_{2F}} \times \int_0^\infty \Sigma_I^{loc} ds \right] = \left[\Gamma - \frac{2\epsilon}{\hbar v_{2F}} \int_0^\infty \Sigma_I^{loc} ds \right]. \quad (76)$$

Since $|\Sigma_1| \sim |\Sigma_I^{loc}| \sim \Gamma$, the pole of the coefficient C is located at small energies $\epsilon \lesssim \Gamma^2/\Delta \ll \Gamma$. Hence, for $\epsilon \ll \Gamma$, the expression for this coefficient takes the form

$$C \left[\epsilon - \epsilon_2(b) + \frac{2}{\xi_{2D}} \int_0^\infty (\Sigma_1 - \Sigma_I^{loc}) ds \right] = \Gamma. \quad (77)$$

The localized self-energies Σ_1 and Σ_I^{loc} can be neglected for $\epsilon \sim \Gamma$. They also vanish for $|b| \gg \xi_S$. In both these limits, Eq. (76) transforms into Eq. (46). The integral term in the equation above can be written in terms of its real, $\beta(b) = \beta_I(b) - \beta_1(b)$, and imaginary, $\gamma(b) = \gamma_I(b) - \gamma_1(b)$, parts as

$$\frac{2}{\xi_{2D}} \int_0^\infty (\Sigma_1 - \Sigma_I^{loc}) ds = -\beta(b) \pm i\gamma(b), \quad (78)$$

where the upper (lower) sign corresponds to the retarded (advanced) Green's function. We next calculate the terms of the real ($\beta_{1,I}$) and imaginary ($\gamma_{1,I}$) parts of integral (78), which are defined by the expressions

$$\beta_\alpha(b) = \frac{2}{\xi_{2D}} \int_0^\infty \text{Re} \Sigma_\alpha(s) ds,$$

$$\gamma_\alpha(b) = \frac{2}{\xi_{2D}} \int_0^\infty \text{Im} \Sigma_\alpha(s) ds$$

and play the respective roles of energy shifting and spectral branch broadening

$$N_\epsilon(s, b) = \frac{\Gamma\gamma(b) \exp(-|s|/\xi_{2D})}{[\epsilon - \epsilon_2(b) - \beta(b)]^2 + \gamma^2(b)}. \quad (79)$$

Since parameters $\beta, \gamma \sim \Gamma/\Delta$ and $\epsilon_2(b)/\Gamma \ll 1$ are small for $b \ll \xi_{2D}$ and $|\epsilon| > \Gamma$, the LDOS reaches its bulk value in this region:

$$N(\rho, \epsilon) = \frac{\sqrt{\epsilon^2 - \Gamma^2}}{|\epsilon|}. \quad (80)$$

Skipping the standard calculations of integrals (78), we give the final expressions for the parameters (see Appendix for the details):

$$\beta = \left\langle \frac{\Gamma^2 \pi q_v}{Q\Omega} \text{sign}(\epsilon + \Omega b) \right\rangle_z,$$

$$\gamma = \left\langle \frac{\Gamma^2 q_v}{Q\Omega} \ln \frac{\Delta_\infty}{|\Omega b + \epsilon|} \right\rangle_z. \quad (81)$$

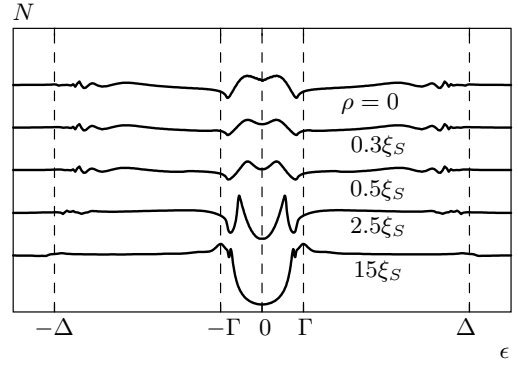


Fig. 8. LDOS in a logarithmic scale for incoherent tunneling in the clean limit. The curves, taken for different distances ρ from the vortex center, are vertically shifted for clarity. The peaks in LDOS exist up to distances $\sim \xi_{2D}$. Here, $\Delta/\Gamma = 5$ and $q_v = 1$

The angular brackets denote averaging over the momentum Q_z along the vortex axis in the bulk, $\Omega = \partial\epsilon_0/\partial b$. The DOS has a peak of height Γ/γ at an energy $\epsilon = \epsilon_2(b) + \beta(b)$ shifted from the standard bound state level. This shift results in a splitting of the zero-bias anomaly [36] (Fig. 8). For calculations, we use a numerical procedure similar to that used earlier for the coherent limit; the induced potentials were averaged over the cylindrical Fermi surface in the bulk.

6.2. Multiple core. Dirty SC with a clean 2D layer

Smearing of the energy dependence of the induced potentials caused by disorder becomes even stronger if the bulk SC has a short mean free path $\ell \ll \xi_S$. In the dirty limit, the momentum-averaged retarded (advanced) Green's functions are parameterized as

$$\check{g}_S^{R(A)}(\rho) = \check{\tau}_3 \sin \Theta^{R(A)} + \check{\tau}_2 \cos \Theta^{R(A)} \exp(-i\check{\tau}_3\phi). \quad (82)$$

We put $\Theta^{R(A)} = \pm\Theta_1 + i\Theta_2$. The boundary conditions for $\rho \rightarrow 0$ are $g^{R(A)} \rightarrow \pm 1$ and $f^{R(A)}, f^{\dagger R(A)} \rightarrow 0$, which requires $\Theta_1 \rightarrow \pi/2$ and $\Theta_2 \rightarrow 0$. At large distances, $\Theta_1 \rightarrow 0$, th $\Theta_2 \rightarrow -\epsilon/\Delta_\infty$ for $\epsilon < \Delta_\infty$ while $\Theta_1 \rightarrow \pi/2$, th $\Theta_2 \rightarrow -\Delta_\infty/\epsilon$ for $\epsilon > \Delta_\infty$. Then, $\Theta_2 = 0$ for $\epsilon \ll \Delta_\infty$, and the Usadel equation becomes [37]

$$D_S \left[\nabla^2 \Theta_1 + \frac{\sin(2\Theta_1)}{2\rho^2} \right] - 2\Delta_0 \sin \Theta_1 = 0. \quad (83)$$

The solution of Eq. (83) was found in Ref. [37]: $\Theta_1(\rho)$ monotonically decays from $\pi/2$ at the origin down to

zero at $\rho \gg \xi_S$. The Green's functions (82) determine the induced vortex potentials $\check{\Sigma}_T = i\Gamma\check{g}_S$.

For small impact parameter values $b \ll \xi_S$, we obtain $\Sigma_I^{loc} = 0$ and the matching condition takes the form

$$\xi_{2D}\theta(s_0) = 2i\zeta(s_0) \int_0^\infty \sin \Theta ds + 2ig(s_0)b \ln \frac{s_0}{\xi_S}. \quad (84)$$

The coefficient C in this case has the only broadened pole at $\epsilon = \epsilon_2(b)$:

$$C[\epsilon - \epsilon_2(b) + i\gamma] = \Gamma \quad (85)$$

with the broadening

$$\gamma = \frac{2\Gamma\sqrt{\Gamma^2 - \epsilon^2}}{\hbar v_{2F}} \int_0^\infty \sin \Theta ds,$$

where the integral is taken along the trajectory. For $|\epsilon| < \Gamma$ and $\rho < \xi_S$, the angle-resolved DOS can be written in the form

$$N_\epsilon(s, b) = \frac{\Gamma^2}{\sqrt{\Gamma^2 - \epsilon^2}} \frac{\gamma(b)e^{-\lambda|s|}}{[\epsilon - \epsilon_2(b)]^2 + \gamma^2(b)}. \quad (86)$$

Consequently, the LDOS has a peak of the height $\sim \Gamma/\gamma(\rho)$ at the energy $\epsilon = \epsilon_2(\rho)$.

For the energies above the induced gap, $\epsilon > \Gamma$, and small impact parameter values $\epsilon_2(b), \gamma(b) \ll \Gamma$, the local DOS can be replaced by its bulk value:

$$N(\rho, \epsilon) = \frac{\sqrt{\epsilon^2 - \Gamma^2}}{|\epsilon|}. \quad (87)$$

For $b \gg \xi_S$, the imaginary part of energy decays exponentially, and Eq. (85) transforms into Eq. (46).

The numerical results shown in Fig. 9 clearly demonstrate the broad peak in the LDOS; this peak shifts and becomes sharper as the distance from the vortex center increases. For $\rho \gg \xi_S$, the LDOS approaches that obtained in the clean limit in Figs. 6 and 8. In calculations, we used the standard relaxation method [38] for solving the Usadel equation in the bulk and the Riccati parameterization for Eilenberger equations in the 2D layer.

6.3. Vortex core expansion. Dirty SC and 2D layer

To complete our analysis, we briefly discuss the case of strong disorder both in the bulk SC and in the 2D layer. In this limit, our model reduces to the one studied numerically in Ref. [39]. The condition

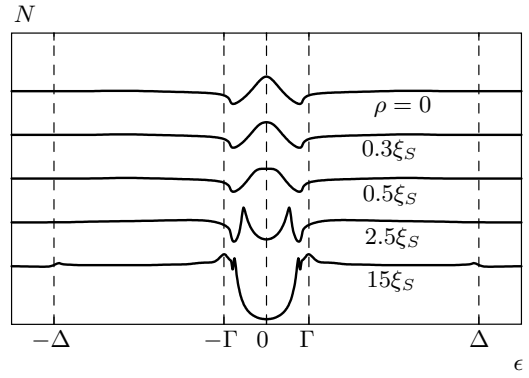


Fig. 9. The local DOS in a logarithmic scale for the dirty limit with the parameters $\Delta/\Gamma = 5$ and $v_{2F}/V_F = 1$. The curves, taken for different distances ρ from the vortex center, are vertically shifted for clarity

$\xi_S \ll \xi_{2D} = \sqrt{\hbar D_{2D}/\Gamma}$ ensures that the short-distance inhomogeneity in the induced vortex potentials inside the primary core region does not disturb the adiabatic solution based on Eq. (25). Indeed, for momentum-orientation-averaged Green's functions in the 2D layer,

$$\check{g}(\rho) = \begin{pmatrix} g_2 & f_2 e^{i\phi} \\ -f_2^\dagger e^{-i\phi} & \bar{g}_2 \end{pmatrix} = \int \frac{d^2 k}{(2\pi)^2} \check{g}(\mathbf{k}, \mathbf{r}),$$

we can derive the equation

$$iD_{2D} [g_2(\nabla^2 - \rho^{-2})f_2 - f_2\nabla^2 g_2] - 2(\epsilon + \Sigma_1)f_2 + 2\check{\Sigma}_2 g_2 = 0, \quad (88)$$

with $\check{\Sigma}_2 = \Sigma_2 e^{-i\phi}$. This equation is similar to that derived by Kupriyanov [40] for a contact of two dirty SCs.

Using a standard parameterization

$$\check{g}(\rho) = \tau_3 \sin \Psi + \tau_2 \cos \Psi \exp(-i\tau_3 \phi)$$

and the expressions for the vortex potentials, we can obtain the equation

$$iD_{2D} \left[\nabla_\rho^2 \Psi - \frac{\sin 2\Psi}{2\rho^2} \right] - 2\Gamma \sin(\Psi - \Theta) - 2i\epsilon \cos \Psi = 0, \quad (89)$$

where $\nabla^2 = \rho^{-1}\partial_\rho(\rho\partial_\rho)$ and $D_{2D} = \hbar v_{2F}^2 \tau/2$ — is the 2D diffusion coefficient. Integrating Eq. (89), multiplied by ρ , in a small region around the origin (from

$\rho = 0$ to a value $\xi_S \ll \rho_0 \ll \xi_{2D}$), we find the matching condition for the adiabatic Green's function (41), (42):

$$D_{2D} \left[\rho \frac{\partial}{\partial \rho} \Psi \Big|_0^{\rho_0} + \int_0^{\rho_0} \frac{\sin 2\Psi}{2\rho} d\rho \right] - 2 \int_0^{\rho_0} \rho d\rho [\Gamma \sin(\Psi - \Theta) + i\epsilon \cos \Psi] = 0. \quad (90)$$

Considering the expansion $\Psi(\rho_0) = \Psi_0 - K\rho_0$ with $K = \partial\Psi(\rho_0)/\partial\rho \sim \xi_{2D}^{-1}$ and assuming $\Psi_0 \neq \pi/2$, we obtain $\cos \Psi_0 \approx \rho_0^2/(\xi_{2D}^2 \ln(\rho_0/\xi_S)) \ll 1$. This estimate confirms the conclusion that the LDOS in the dirty limit follows the bulk LDOS pattern scaled with the 2D coherence length ξ_{2D} to within the second-order terms in the small parameter ρ_0/ξ_{2D} .

The resulting problem at low energies $\epsilon \ll \Delta_\infty$ coincides with that of describing a standard vortex in a dirty SC [41] with the gap value Γ . Hence, the full disordered system should reveal the same LDOS patterns as in the bulk case, albeit scaled with the much larger coherence length ξ_{2D} instead of ξ_S . This vortex-core expansion can account for anomalously large vortex images observed in MgB₂ [42] and in high- T_c cuprates [43].

7. DISCUSSION

The results described above imply that the electron states in the induced superconducting configurations strongly depend on the tunneling mechanism and on the crystal structure of bulk and 2D materials. The structure and symmetry of electron states can be essentially different from those in the bulk SC. This imposes severe restrictions on possible realizations of various exotic proximity electron states [30, 31] including Majorana states [9] and, in particular, Majorana states in the vortex cores. Our results directly show that the existence of zero-energy states in the proximity-induced vortex core crucially depends on the tunneling mechanism underlying the proximity coupling between the 2D layer and the bulk SC. The zero-energy core state can be expected to exist for coherent tunneling between the SC and the 2D layer that both have isotropic Fermi surfaces, if the symmetry of the induced superconducting order permits.

It is known that a zero-energy core state exists for a vortex with an odd vorticity in a graphene monolayer with intrinsic superconductivity [44–46]. The graphene monolayer with proximity-induced superconductivity thus would seem to be a good candidate to look for a zero-energy state. But the Fermi surface of graphene is

highly anisotropic; it lies near the Dirac corners of the Brillouin zone with the group velocity directed radially from the Dirac points. This group velocity direction does not coincide with the direction of the Fermi momentum and of the Fermi velocity in the bulk SC, as is shown in Fig. 7. Although the results in the previous sections were obtained within the QC approximation, they still can shed a light on the possibility of the zero-energy state in graphene, especially for a sufficient doping level when the QC approximation for graphene is justified [46]. In this case, the results in Sec. 5.2 can be applied. They show that each state in the induced vortex core with energy ϵ is coupled to an infinite set of levels in the primary core. The integral I_{odd} accounts for these states. Its real part deals with off-resonance states with eigen-energies not equal to ϵ , while the imaginary part comes from the resonance state with the same eigen-energy ϵ . According to Sec. 5.2, the real part of I_{odd} disappears for $\epsilon = 0$ and $b = 0$. The fate of the imaginary part depends on whether the zero energy is in resonance with any state in the primary core. It is known that for an s -wave clean bulk superconductor, the core levels are discrete with a minigap $\omega_0 \sim \Delta^2/E_F$ and no one lies at zero energy. Therefore, if the levels in the bulk are not broadened by disorder or by inelastic scattering, the imaginary part of I_{odd} does not appear, and the zero-energy state seems to be intact. The discrete nature of the core states is, of course, beyond the QC approximation. Therefore, the above consideration gives only a hint towards the possibility of a zero-energy state. The detailed analysis is needed that would be based on the rigorous quantum mechanical description. We note that an alternative possibility to save the zero-energy states by introducing a cylindrical cavity in the bulk superconductor was considered in Refs. [25, 26].

Another important feature of induced superconductivity in a LD system is an extremely large coherence length ξ_{2D} . It provides a unique possibility to realize vortex configurations with quite unusual parameters. Here, we briefly discuss some configurations that are of interest. The detailed analysis of all these situations requires special considerations. First of all, we note that the results in Secs. 3 and 5 and the subsequent sections are valid for $\xi_{2D} \ll \min(r_v, \lambda_L)$, where r_v is the intervortex distance and λ_L is the London penetration length in the bulk SC. If the vortex lattice in the bulk SC is sufficiently dense with the intervortex distance $\xi_{2D} \lesssim r_v \ll \lambda_L$, the induced 2D vortex cores may start to overlap. The spectrum ϵ_2 is then modified due to intervortex tunneling of QPs [47]. The effect of the intervortex QP tunneling should be im-

portant if the splitting of the quantized energy levels due to this tunneling exceeds the minigap value. The splitting can be estimated as $\Gamma \exp[-r_v/\xi_{2D}]$ while the minigap inside the induced vortex core is of the order of $\Gamma^2/\hbar v_{2F} k_{2F}$. Thus, the ratio determining the intervortex tunneling efficiency is an exponential with a large prefactor, $\hbar v_{2F} k_{2F} \Gamma^{-1} \exp[-r_v/\xi_{2D}]$. Just this ratio controls the interplay between the velocity of the trajectory precession and the QP tunneling rate. The changes in the QP spectrum become essential when $r_v \lesssim \xi_{2D} \ln(\hbar v_{2F} k_{2F}/\Gamma)$. The minigap in this case should vanish according to the analysis in Ref. [47].

In some cases, the 2D coherence length ξ_{2D} can exceed the London penetration depth λ_L ; this depends on the properties of the bulk SC and on the tunneling rate Γ . If $\xi_{2D}, r_v \gg \lambda_L$, the superconducting velocity vanishes along the trajectories with $b > \lambda_L$, and hence the spectral branch $\epsilon_2(b)$ saturates already for $b \sim \lambda_L$.

Our results for coherent tunneling can be directly generalized to clean d -wave bulk SCs with isotropic Fermi surfaces. However, the incoherent tunneling destroys the superconducting coherence in the 2D layer. As a result, the branch ϵ_2 disappears, while the QP states for $\epsilon < \Delta$ have finite lifetimes for distances close to the vortex cores in the bulk SC.

Considering possible experimental realizations of the induced vortex states, one has to bear the finite dimensions L of the 2D layer in mind. The large size of the induced vortex cores can lead to the situation typical for mesoscopic superconducting samples when L is close to several ξ_{2D} s. The criterion for the vortex spectrum transformation caused by the boundary effects in such systems to become important can be found using the results in Ref. [48]. We only need to replace the gap, the coherence length, and the minigap by the appropriate values in the 2D layer. The criterion appears to be very similar to that describing the efficiency of intervortex tunneling: the mesoscopic fluctuations of quantum levels in the 2D core become comparable with the minigap for $L \lesssim \xi_{2D} \ln(\hbar v_{2F} k_{2F}/\Gamma)$.

In conclusion, the model of a proximity-coupled 2D layer allows theoretically studying many spatially inhomogeneous situations including various configurations of induced vortices. Based on this model, we have presented a description of the vortex core states for some typical tunneling mechanisms. In particular, our results can be used for interpreting the STM data on the vortex LDOS in superconductors through the model of a thin proximity layer present at the surface of the bulk SC. The effect of a thin non-superconducting proximity layer can explain various experimentally observed features of the vortex LDOS and reveals

that the STM technique alone is not sufficient for identifying a multicomponent or anisotropic energy gap.

We thank A. Buzdin, G. Volovik and A. Smirnov for the stimulating discussions. This work was supported in part by EU 7th Framework Programme (FP7/2007-2013) under Grant agreements No. 228464 (Microkelvin) and No. 308850, by the Academy of Finland through its LTQ CoE grant (project no. 250280), by the Russian Foundation for Basic Research (grant No. 12-02-00421), by the Program ‘‘Quantum Physics of Condensed Matter’’ of the Russian Academy of Sciences, by the Russian president foundation (SP-1491.2012.5), and by Federal Target Program ‘‘Scientific and educational personnel of innovative Russia in 2009–2013’’.

APPENDIX

Calculation of self-energies for incoherent tunneling

In this Appendix, we calculate the following integrals from the main text:

$$\beta_\alpha(b) = \frac{2}{\xi_{2D}} \int_0^\infty \text{Re} \Sigma_\alpha(s) ds,$$

$$\gamma_\alpha(b) = \frac{2}{\xi_{2D}} \int_0^\infty \text{Im} \Sigma_\alpha(s) ds.$$

For this, we consider the case of the small impact parameter values $b \ll \xi_S$:

$$\beta_I(b) = \frac{2\Gamma^2 b}{v_{2F}} \int_0^\infty \left\langle \frac{v_{\parallel} e^{-K}}{2Q\Omega\rho^2} \times \left[1 - \text{Re} \frac{|\epsilon|}{\sqrt{\epsilon^2 - \Omega^2 \rho^2}} \right] \right\rangle_z ds,$$

where $\rho^2 = b^2 + s^2$. In this case, the first term in the above integral is determined by $s \sim b$:

$$\begin{aligned} \Gamma b \int_0^\infty \left\langle \frac{v_{\parallel} e^{-K}}{Q\Omega\rho^2} \right\rangle_z ds &= \Gamma b \int_0^\infty \left\langle \frac{v_{\parallel}}{Q\Omega(s^2 + b^2)} \right\rangle_z ds = \\ &= \text{sign}(b) \Gamma \left\langle \frac{\pi v_{\parallel}}{2Q\Omega} \right\rangle_z. \end{aligned}$$

The second term is determined by very small impact parameters and is given by

$$\int_0^{b_0} \frac{ds}{\sqrt{b_0^2 - s^2}} = \frac{\pi}{2}, \quad \int_0^{b_0} \frac{ds}{(s^2 + b_0^2)\sqrt{b_0^2 - s^2}} = \frac{\pi\Omega}{2|b\epsilon|},$$

where $b_0^2 = \epsilon^2/\Omega^2 - b^2 > 0$. As a result, we find

$$\beta_I(b) = \text{sign}(b) \frac{\Gamma^2}{v_{2F}} \left\langle \frac{\pi v_{\parallel}}{Q\Omega} \chi(\Omega^2 b^2 - \epsilon^2) \right\rangle_z,$$

$$\beta_1(b) = -\text{sign}(\epsilon) \frac{\Gamma^2}{v_{2F}} \left\langle \frac{\pi v_{\parallel}}{Q\Omega} \chi(\epsilon^2 - \Omega^2 b^2) \right\rangle_z,$$

where $\chi(x)$ is the Heaviside theta function, i.e., $\chi(x) = 1$ for $x > 0$ and $\chi(x) = 0$ for $x < 0$.

After simplifying the expression for $\beta(b) = \beta_I(b) - \beta_1(b)$, we obtain Eq. (81). For $b \gtrsim \xi_S$, the quantity $\beta(b)$ decays as $\exp(-2b/\xi_S)$.

The expressions for imaginary parts hold for any distances ρ because the delta functions in the integrals select only the trajectories that pass at small impact parameters:

$$\begin{aligned} \gamma_1(b) &= \frac{\Gamma^2}{v_{2F}} \int_0^{\infty} \left\langle \frac{v_{\parallel} e^{-K}}{Q\sqrt{\Omega^2 \rho^2 - \epsilon^2}} \chi(\Omega^2 \rho^2 - \epsilon^2) \right\rangle_z ds = \\ &= \frac{\Gamma^2}{v_{2F}} \left\langle \frac{v_{\parallel}}{Q\Omega} \ln \frac{\Delta_{\infty}}{\sqrt{|\Omega^2 b^2 - \epsilon^2|}} \right\rangle_z, \end{aligned}$$

$$\begin{aligned} \gamma_I(b) &= \frac{\Gamma^2 b}{v_{2F}} \times \\ &\times \int_0^{\infty} \left\langle \frac{\epsilon}{\Omega \rho^2} \frac{v_{\parallel} e^{-K}}{Q\sqrt{\Omega^2 \rho^2 - \epsilon^2}} \chi(\Omega^2 \rho^2 - \epsilon^2) \right\rangle_z ds = \\ &= \text{sign}(b\epsilon) \frac{\Gamma^2}{v_{2F}} \left\langle \frac{v_{\parallel}}{Q\Omega} \ln \frac{\Omega|b| + |\epsilon|}{\sqrt{|\Omega^2 b^2 - \epsilon^2|}} \right\rangle_z. \end{aligned}$$

We here use the following expressions for the standard integrals:

$$\int_{b_0}^{s_{max}} \frac{ds}{\sqrt{s^2 \pm b_0^2}} = \ln \frac{\Delta}{\sqrt{|\Omega^2 b^2 - \epsilon^2|}},$$

where $s_{max} \sim \xi_S$, and

$$\int_{b_0}^{s_{max}} \frac{ds}{\sqrt{s^2 \pm b_0^2}(s^2 + b^2)} = \frac{\Omega}{|b\epsilon|} \ln \frac{\Omega|b| + |\epsilon|}{\sqrt{|\Omega^2 b^2 - \epsilon^2|}}.$$

The imaginary terms also decay exponentially for $b \gtrsim \xi_S$. The expression for $\gamma(b) = \gamma_1(b) - \gamma_I(b)$ gives Eq. (81).

REFERENCES

1. W. L. McMillan, *Phys. Rev.* **175**, 537 (1968).
2. P. G. de Gennes, *Superconductivity of Metals and Alloys*, Addison-Wesley, New York (1989).
3. C. W. J. Beenakker, *Rev. Mod. Phys.* **80**, 1337 (2008).
4. A. H. Castro Neto, F. Guinea, N. M. Peres, K. S. Novoselov, and A. K. Geim, *Rev. Mod. Phys.* **81**, 109 (2009).
5. M. Kociak, A. Yu. Kasumov, S. Guéron, B. Reulet, I. I. Khodos, Yu. B. Gorbatov, V. T. Volkov, L. Vaccarini, and H. Bouchiat, *Phys. Rev. Lett.* **86**, 2416 (2001).
6. J. C. Charlier, X. Blase, and S. Roche, *Rev. Mod. Phys.* **79**, 677 (2007).
7. Xiao-Liang Qi and Shou-Cheng Zhang, *Rev. Mod. Phys.* **83**, 1057 (2011).
8. H. B. Heersche, P. Jarillo-Herrero, J. B. Oostinga, L. M. K. Vandersypen, and A. F. Morpurgo, *Sol. St. Comm.* **143**, 72 (2007);
9. L. Fu and C. L. Kane, *Phys. Rev. Lett.* **100**, 096407 (2008).
10. J. Alicea, *Rep. Progr. Phys.* **75**, 076501 (2012).
11. H. F. Hess, R. B. Robinson, R. C. Dynes, J. M. Valles, Jr., and J. V. Waszczak, *Phys. Rev. Lett.* **62**, 214 (1989); H. F. Hess, R. B. Robinson, and J. V. Waszczak, *Phys. Rev. Lett.* **64**, 2711 (1990); I. Guillamon, H. Suderow, S. Vieira, L. Cario, P. Diener, and P. Rodiere, *Phys. Rev. Lett.* **101**, 166407 (2008).
12. C. Caroli, P. G. de Gennes, and J. Matricon, *Phys. Lett.* **9**, 307 (1964).
13. A. Kastalsky, A. W. Kleinsasser, L. H. Greene, R. Bhat, F. P. Milliken, and J. P. Harbison, *Phys. Rev. Lett.* **67**, 3026 (1991); D. Quirion, C. Hoffmann, F. Lefloch, and M. Sanquer, *Phys. Rev. B* **65**, 100508(R) (2002).
14. B. J. van Wees, P. de Vries, P. Magnee, and T. M. Klapwijk, *Phys. Rev. Lett.* **69**, 510 (1992).
15. A. F. Volkov, *Pis'ma Zh. Eksp. Teor. Fiz.* **55**, 713 (1992) [*JETP Lett.* **55**, 746 (1992)]; *Physica B* **203**, 267 (1994).

16. A. F. Volkov, P. H. C. Magnée, B. J. van Wees, and T. M. Klapwijk, *Physica C* **242**, 261 (1995).
17. F. W. J. Hekking and Yu. V. Nazarov, *Phys. Rev. B* **49**, 6847 (1994).
18. N. B. Kopnin, *Phys. Rev. B* **57**, 11775 (1998); A. S. Mel'nikov, *Phys. Rev. Lett.* **86**, 4108 (2001).
19. Ø. Fischer, M. Kugler, I. Maggio-Aprile, C. Berthod, and Ch. Renner, *Rev. Mod. Phys.* **79**, 353 (2007).
20. A. E. Koshelev and A. A. Golubov, *Phys. Rev. Lett.* **90**, 177002 (2003).
21. F. Giubileo, D. Roditchev, W. Sacks, R. Lamy, D. X. Thanh, J. Klein, S. Miraglia, D. Fruchart, J. Marcus, and Ph. Monod, *Phys. Rev. Lett.* **87**, 177008 (2001).
22. N. B. Kopnin and A. S. Melnikov, *Phys. Rev. B* **84**, 064524 (2011).
23. G. Fagas, G. Tkachov, A. Pfund, and K. Richter, *Phys. Rev. B* **71**, 224510 (2005).
24. J. D. Sau, R. M. Lutchyn, S. Tewari, and S. DasSarma, *Phys. Rev. B* **82**, 094522 (2010).
25. A. L. Rakhmanov, A. V. Rozhkov, and Franco Nori, *Phys. Rev. B* **84**, 075141 (2011); R. S. Akzyanov, A. V. Roshkov, A. L. Rakhmanov, and F. Nori, arXiv: cond-mat/1307.0923.
26. P. A. Iosevich, P. M. Ostrovsky, and M. V. Feigelman, *Phys. Rev. B* **86**, 035441 (2012).
27. N. B. Kopnin, *Theory of Nonequilibrium Superconductivity*, Oxford (2001).
28. A. A. Abrikosov, L. P. Gor'kov, and I. E. Dzyaloshinskii, *Metody Kvantovoj Teorii Polya v Statisticheskoi Fizike*, Fizmatgiz (1962) [*Quantum Field Theoretical Methods in Statistical Physics*, Pergamon (1965)].
29. C. W. J. Beenakker, *Phys. Rev. Lett.* **97**, 067007 (2006).
30. Y. Oreg, G. Refael, and F. von Oppen, *Phys. Rev. Lett.* **105**, 177002 (2010).
31. E. Peretto, *Phys. Rev. Lett.* **110**, 087001 (2013).
32. L. Kramer and W. Pesch, *Z. Phys.* **269**, 59 (1974).
33. G. E. Volovik, *Pis'ma Zh. Eksp. Teor. Fiz.* **57**, 233 (1993) [*JETP Lett.* **57**, 244 (1993)]; *The Universe in a Helium Droplet*, Oxford Univ. Press (2003).
34. K. Shiozaki, T. Fukui, and S. Fujimoto, *Phys. Rev. B* **86**, 125405 (2012).
35. N. Schopohl and K. Maki, *Phys. Rev. B* **52**, 490 (1995).
36. I. Maggio-Aprile, Ch. Renner, A. Erb, E. Walker, and Ø. Fischer, *Phys. Rev. Lett.* **75**, 2754 (1995); B. W. Hoogenboom, Ch. Renner, B. Revaz, I. Maggio-Aprile, and Ø. Fischer, *Physica C* **332**, 440 (2000); S. H. Pan, E. W. Hudson, A. K. Gupta, K.-W. Ng, H. Eisaki, S. Uchida, and J. C. Davis, *Phys. Rev. Lett.* **85**, 1536 (2000).
37. L. P. Gor'kov and N. B. Kopnin, *Zh. Eksp. Teor. Fiz.* **65**, 396 (1973) [*Sov. Phys. JETP* **38**, 195 (1974)].
38. A. Berman, and R. J. Plemmons, *Nonnegative Matrices in the Mathematical Sciences*, SIAM (1994).
39. A. A. Golubov, *Czechoslovak Journal of Physics* **46**, 569 (1996).
40. M. Yu. Kupriyanov, *Sverhprovodimost': Fizika, Khimija, Tekhnika* **2**, 5 (1989).
41. A. A. Golubov and U. Hartmann, *Phys. Rev. Lett.* **72**, 3602 (1994).
42. M. R. Eskildsen, M. Kugler, S. Tanaka, J. Jun, S. M. Kazakov, J. Karpinski, and Ø. Fischer, *Phys. Rev. Lett.* **89**, 187003 (2002).
43. A. D. Beyer, M. S. Grinolds, M. L. Teague, S. Tajima, and N.-C. Yeh, *Europhys. Lett.* **87**, 37005 (2009).
44. R. Jackiw and P. Rossi, *Nucl. Phys. B* **190**, 681 (1981).
45. D. L. Bergman and K. L. Hur, arXiv:cond-mat/0806.0379.
46. I. M. Khaymovich, N. B. Kopnin, A. S. Mel'nikov, and I. A. Shereshevskii, *Phys. Rev. B* **79**, 224506 (2009).
47. A. S. Mel'nikov and M. A. Silaev, *Pis'ma Zh. Eksp. Teor. Fiz.* **83**, 675 (2006) [*JETP Lett.* **83**, 578 (2006)].
48. N. B. Kopnin, A. S. Mel'nikov, V. I. Pozdnyakova, D. A. Ryzhov, I. A. Shereshevskii, and V. M. Vinokur, *Phys. Rev. Lett.* **95**, 197002 (2005); A. S. Mel'nikov, D. A. Ryzhov, and M. A. Silaev, *Phys. Rev. B* **78**, 064513 (2008).